

Sucrose Non-Fermenting Related Kinase Enzyme Mediated Rho-Associated Kinase Signaling is Responsible for Cardiac Function

Running title: *Cossette et al.; SNRK-ROCK cardiac function*

Stephanie M. Cossette, PhD¹; Vijesh J. Bhute, BTech³; Xiaoping Bao, PhD³; Leanne M. Harmann, BA²; Mark A. Horswill, MS⁴; Indranil Sinha, PhD⁵; Adam Gastonguay, PhD¹; Shabnam Pooya, PhD¹; Michelle Bordas, BS¹; Suresh N. Kumar, PhD⁶; Shama P. Mirza, PhD⁸; Sean Palecek, PhD³; Jennifer Strande, MD, PhD⁷; Ramani Ramchandran, PhD^{1,9}

¹Department of Pediatrics, ⁹OBGYN, Medical College of Wisconsin, Developmental Vascular Biology Program, Children's Research Institute; ²Division of Cardiovascular Medicine, Cardiovascular Center, Clinical and Translational Science Institute, ⁷Division of Cardiovascular Medicine, Department of Cell Biology, Neurobiology and Anatomy, Cardiovascular Center, Clinical and Translational Science Institute, ⁶Division of Pediatric Pathology, Department of Pathology, Medical College of Wisconsin, Milwaukee; ³Department of Chemical and Biological Engineering, ⁴Morgridge Institute for Research, University of Wisconsin-Madison, Madison, WI; ⁵Marginalen Bank, Stockholm, Sweden; ⁸Department of Chemistry and Biochemistry, University of Wisconsin-Milwaukee, Milwaukee, WI

Correspondence:

Ramani Ramchandran, PhD

Department of Pediatrics

Medical College of Wisconsin

CRI Developmental Vascular Biology Program, C3420

8701 Watertown Plank Road, P.O. Box 26509

Milwaukee, WI 53226

Tel: 414-955-2387

Fax: 414-955-6325

E-mail: rramchan@mcw.edu

Journal Subject Terms: Basic Science Research; Myocardial Biology; Mechanisms; Proteomics; Metabolism

Abstract:

Background - Cardiac metabolism is critical for the functioning of the heart, and disturbance in this homeostasis is likely to influence cardiac disorders or cardiomyopathy. Our lab has previously shown that sucrose non-fermenting related kinase (SNRK) enzyme, which belongs to the AMP-activated kinase (AMPK) family, was essential for cardiac metabolism in mammals.

Snrk global homozygous knockout (KO) mice die at postnatal day 0, and conditional deletion of *Snrk* in cardiomyocytes (*Snrk* cmcKO) leads to cardiac failure, and death by 8-10 months.

Methods and Results - We performed additional cardiac functional studies using echocardiography (ECHO), and identified further cardiac functional deficits in *Snrk* cmcKO mice. NMR-based metabolomics analysis identified key metabolic pathway deficits in *SNRK* knockdown cardiomyocytes (CMs) *in vitro*. Specifically, metabolites involved in lipid metabolism and oxidative phosphorylation are altered and perturbations in these pathways can result in cardiac function deficits and heart failure. A phosphopeptide-based proteomic screen identified Rho-associated kinase (ROCK) as a putative substrate for SNRK and mass spec-based fragment analysis confirmed key amino acid residues on ROCK that are phosphorylated by SNRK. Western blot analysis on heart lysates from *Snrk* cmcKO adult mice and *SNRK* knockdown CMs showed increased ROCK activity. In addition, *in vivo* inhibition of ROCK partially rescued the *in vivo* *Snrk* cmcKO cardiac function deficits.

Conclusions - Collectively, our data suggests that SNRK in CMs is responsible for maintaining cardiac metabolic homeostasis, which is mediated in part by ROCK and alteration of this homeostasis influences cardiac function in the adult heart.

Key words: metabolism; cardiac; Rho-associated kinases; echocardiography; SNRK, MYH6

Introduction

Cardiomyopathy is a complex disorder influenced by several factors. Some of these factors include impaired endothelial function and sensitivity to various ligands (β -agonists), altered intracellular calcium homeostasis, and accumulation of connective tissue such as insoluble collagen¹. Recently, cardiomyopathy as a consequence of early alterations in cardiac metabolism has been proposed, particularly with respect to diabetes². A potential link between cardiac metabolism and function is the Ras homolog family member A (RhoA)-associated kinase (ROCK) signaling pathway. The RhoA/ROCK signaling pathway has been implicated in several cardiovascular and metabolic disorders such as atherosclerosis, cardiac hypertrophy and diabetes³. ROCK is a serine threonine kinase involved in regulating various cellular processes such as cell contraction, migration, proliferation, apoptosis/survival and gene expression/differentiation⁴. Interestingly, pharmacological inhibition of RhoA/ROCK activity has been shown to improve cardiac function in diabetes-induced cardiomyopathy⁵. To date signaling molecules regulating ROCK activity have primarily been restricted to the RhoA pathway. Our lab has identified a novel member of the AMP-activated kinase (AMPK) family namely sucrose non-fermenting related kinase (SNRK) that is essential for angiogenesis⁶, and responsible for cardiac metabolism in mammals⁷. Here, we implicate SNRK as a putative regulator of ROCK activity in cardiomyocytes (CMs).

CMs metabolism is developmentally dynamic in that the fetal heart primarily utilizes glucose as its major energy substrate, and during postnatal maturation, the heart switches to primarily utilizing fatty acid oxidation to meet its energy demands^{8,9}. In our previous work⁷, we reported that the global *Snrk* KO mice die within 24 hours after birth, displayed enlarged hearts, and lethality is associated with metabolic defects in cardiac tissues. SNRK maintains metabolic

homeostasis via regulation of the phosphorylated acetyl-coA carboxylase (pACC)-phosphorylated AMPK (pAMPK) pathway during this transitional period in development⁷. Furthermore, cardiac specific conditional *Snrk* KO (*Snrk* cmcKO) adult mice display severe cardiac functional deficits and lethality within 8-10 months. We extend this work further in this study, and identified ROCK as a putative substrate for SNRK that contributes to this metabolic deficit in the heart. NMR-based metabolomics in human embryonic stem cell derived-CMs and signaling studies in both adult heart lysates and cultured CMs collectively imply that SNRK-mediated ROCK signaling pathway is an important regulator of cardiac function in mammals.

Methods

Detailed methods are described in the Supplemental Materials.

Fasudil Rescue

Male and female mice between six and four months of age were given fasudil (10mg/kg) or saline daily for 28 days via intraperitoneal injections. ECHO analysis was performed immediately prior to the initial injection and ECHO imaging was repeated at 14 and 28 days. At the end of the experiment the mice were euthanized using CO₂ and cervical dislocation as per the approved IACUC animal protocol.

Metabolomics Analysis

CMs treated with either non-silencing shRNA control or shSNRK lentivirus were cultured in RPMI containing B27 (no insulin) for 48 h prior to sample collection. Sample collection and extraction was performed as described previously in Bhute and Palecek¹⁰. ¹H NMR spectra were acquired using standard NOESYPR1D pulse sequence (RD-90°-t1-90°-tm-90°-acquire) with a relaxation delay of 1 s, a mixing time of 100 ms and a pre-scan delay of 30 μs and consisted of 128 transients or free induction decays (FIDs) collected into 48 K complex data points with a



spectral width of 12 ppm and an acquisition time of 4 s. FIDs were zero-filled to 128k data points and multiplied by an exponential window function (LB=0.5Hz). The chemical shifts were referenced to the TMS peak ($\delta=0$ ppm), using TopSpin™ software (version 3.1, Bruker). Spectral processing like phasing, baseline correction and solvent region removal (water and DMSO) was performed using ACD/1D NMR processing (Advanced Chemistry Development). Targeted profiling¹¹ was performed using ChenomX NMR Suite Profiler (version 7.7, ChenomX Inc.) and the concentrations were references to TMS. Peak annotation was performed based on the existing ChenomX library and HMDB¹². The metabolite concentrations were exported to an Excel file for further analysis.

The concentration data matrix was normalized by the total concentration of metabolites, which was equivalent to normalization by total spectral area in each sample to evaluate the metabolite fractions and also to account for the differences in cell number and efficiencies of extraction. Statistical and pathway analysis was performed using MetaboAnalyst 3.0¹³. The concentration data was auto-scaled (mean centering followed by dividing each variable by the standard deviation) prior to principal component analysis (PCA) and student's t-test was performed assuming unequal group variance and α was chosen to be 0.05. Pathway topology analysis was performed in MetaboAnalyst's pathway analysis module using global test algorithm for pathway enrichment (adjusted for multiple testings) and out-degree centrality to assess importance. The *Homo Sapiens* library was used for analysis and the metabolic pathways with an impact score > 0 and FDR <0.05 were considered to be significantly enriched.

Protein Kinase Array

Purified SNRK protein was provided to Invitrogen (Life Technologies) for kinase substrate identification service on ProtoArray human protein microarray. In short, SNRK was assayed at

concentration of 5 nM and 50 nM on ProtoArray human protein microarrays v5.0. All possible kinase substrates at each concentration of SNRK were evaluated by their Z-Factor rank within the array and were compared to the negative control assay. A protein was defined as being a candidate substrate if it met the following conditions: The Z-Factor, or signal-to-noise ratio, was greater than 0.35 on at least one array, indicating a signal greater than 1.5-fold above the noise. The Signal Used value was greater than 2,000 relative units on at least one array probed with SNRK and was greater than 2-fold higher than the Signal Used value for the corresponding protein in the negative control assay. The replicate spot CV was less than 50% on the corresponding array. The inter-assay CV was less than 50%. Additional experimental details are available upon request.



***In vitro* ROCK Phosphorylation Protocol**

Human umbilical vein endothelial cells (HUVECs) (Lonza CC2519) were lysed with RIPA buffer (Sigma) containing complete mini EDTA-free protease inhibitor cocktail (Roche) and PhosSTOP phosphatase inhibitor (Roche). Samples were incubated on ice for 20 mins and cleared at 13,300 rpm at 4°C for 30 mins. ROCK1 was immunoprecipitated using an anti-ROCK1 antibody (Cell Signaling Technology) with protein G agarose beads (Thermo Scientific). Immunoprecipitates were washed 3x with dilution buffer (10 mM Tris, 130 mM NaCl, 0.05% Triton-X-100, 0.1% BSA, protease inhibitors). Additional washes with 50 mM Tris (pH 8.0) and Tris-Saline (10 mM Tris HCl, 140 mM NaCl) (pH 8.0) were also performed. The Lowry quantification method was used to determine the protein concentration.

Immunoprecipitated ROCK1 protein was incubated with or without 5 nM to 30 nM purified SNRK protein in the presence of 3 μ M γ -ATP-32 (Perkin Elmer) and 1 μ M ATP (Cell Biolabs) in kinase buffer [20 mM HEPES (pH7.7), 20 mM MgCl₂, 2 mM DTT, 1X protease inhibitor

(Roche) and 1X phosphatase inhibitor (Roche)]. The samples were allowed to incubate for 15 mins at 30°C. After incubation the samples were washed 2-3 times with kinase buffer and re-suspended in Lamelli sample buffer. 5 µl of the reaction was reserved for radioactive analysis and the remaining samples were resolved on a 10% Mini-PROTEAN TGX precast gel (BioRad) and subjected to SDS-PAGE. The gel was then dried and exposed to autoradiography film.

Western Blot (WB) Analysis

Adult heart tissues were collected immediately after euthanization, and the proteins were isolated using homogenization in RIPA buffer (Sigma) with complete mini EDTA-free protease inhibitor cocktail (Roche) and PhosSTOP phosphatase inhibitor (Roche) using a Qiagen TissueRuptor.

Methodologies related to protein estimation, quantitation were described previously⁷. The following antibodies were used: anti- myosin-binding subunit (MBS; BioLegend), anti-phospho MBS (pMBS; Cell Signaling Technology/MBL International); anti-ROCK1 (BD Bioscience); anti-ROCK2 (BD Bioscience); anti-extracellular signal-regulated kinase (ERK; Cell Signaling Technology); anti-phospho ERK (pERK; Cell Signaling Technology); anti-protein kinase B (AKT; Cell Signaling Technology); anti-phospho AKT (pAKT; Cell Signaling Technology); anti-inhibitor of kappa B kinase (IKK; Cell Signaling Technology); anti-phospho IKK(pIKK; Cell Signaling Technology); anti-Tubulin (Sigma), anti-rabbit horseradish peroxidase (HRP; Cell Signaling Technology) and anti-mouse HRP (Cell Signaling Technology).

Statistics

Student's unpaired t-test was used for comparison analysis for the cardiomyocyte western blot, metabolomics and trichrome staining analysis. Mann-Whitney test was used for comparison analysis for the adult heart western blot analysis and all of the ECHO data analysis. The results are described as means (\pm standard error of the mean, SEM). A p-value of $p < 0.1$ was considered

to be approaching significance. A p-value of $p < 0.05$ was considered significant when comparing two parameters. For all of the *in vivo* and *in vitro* ROCK signaling and inhibitor experiments a p-value of $p < 0.05$ was considered to be slightly significant, and a p-value of $p < 0.0125$ was considered significant due to p-value correction for multiple comparisons. Sample data values for the trichrome staining analysis and the western blot experiments are provided in Table S1. Sample data values for the metabolomics data are provided in Table S2.

Results

***Snrk* cardiac (cmcKO) conditional knockout adult mice show myocardial dysfunction and increased cardiac fibrosis**

Previously, our lab assessed the role of *Snrk* in mammalian development, and concluded that SNRK is essential for cardiac metabolism⁷. In that study, we generated and validated the global and cardiac-specific (MYH6CRE)¹⁴ conditional *Snrk* cmcKO mouse reagents⁷. Homozygous loss of *Snrk* (LoxP/LoxP) in CMs results in lethality between 8-10 months of age and heterozygous loss of *Snrk* (LoxP/WT) showed lethality shortly after one year of age. Echocardiography (ECHO) analysis on 6 month old adult male mice showed significant enlargement of the left ventricle inner diameter (LVID) in systole (s) and diastole (d), significant increase in end diastolic volume (EDV) and end systolic volume (ESV), significant decrease in the ejection fraction (EF) and the fractional shortening (FS) in the *Snrk* cmcKO (MYH6CRE *Snrk*^{LoxP/LoxP}) mice compared to the CRE negative littermates⁷. We now performed strain and strain rate imaging analysis (Fig. 1A), which showed that *Snrk* cmcKO display significantly worsening strain patterns including decreased radial strain ($p=0.0286$), increased circumferential strain ($p=0.0286$), decreased strain rates S ($p=0.0286$). The strain rate changes correlates with a decrease in systolic function. The *Snrk* cmcKO mice also display an increased strain rate E



($p=0.0286$) that is associated with worsening diastolic function. Furthermore, the pulmonary acceleration time (PAT) ($p=0.0571$), ejection time (ET) ($p=0.0571$) (Fig. 1B) and right ventricular outflow tract time velocity-integrals (TVI) were also decreased in *Snrk* cmcKO ($p=0.0571$) (Fig. 1C). All together, these findings are consistent with a dilated cardiomyopathy with a resultant increase in pulmonary artery pressure.

We next investigated whether myocardial stiffening and impaired cardiac function could be the result of increase in extracellular matrix deposition, a phenomenon described as myocardial fibrosis¹⁵. We performed trichrome staining on *Snrk* cmcKO heart tissue sections (Fig. 1D). *Snrk* cmcKO showed a significant increase in fibrosis staining (CRE neg 10.38%, cmcKO 19.32% $p=0.0212$) (Fig. 1E and Table S1). These data indicates deformation in the heart segments resulting in altered myocardial function and suggest that *Snrk* in CMs is critical for maintaining heart contractility.

***SNRK* knockdown CMs *in vitro* show defective metabolism**

To investigate what might be amiss in CMs in the absence of SNRK, we investigated changes in metabolism in *SNRK* knockdown CMs *in vitro* since previous data on *Snrk* cmcKO mice showed cardiac metabolic defects⁷. CMs treated with either non-silencing shRNA control or efficacy-confirmed shSNRK lentivirus was subjected to NMR-based metabolomics measurement as described in the methods section. The heat maps (Fig. 2A) and subsequent graphical representation (Fig. 2B) clearly depict extensive metabolic changes in *SNRK* knockdown CMs. Metabolites that significantly increased (Fig. S1A) and decreased (Fig. S1B) in *SNRK* knockdown CMs have been indicated. Among the increased metabolites, we observed significant increase in multiple osmolytes including glycerophosphocholine (Fold Change: 1.44, $p=0.0046$) and taurine (Fold Change: 1.27, $p=0.038$). We also observed an increase in a few essential amino

acids including valine and threonine while, majority of the non-essential amino acids including alanine ($p < 0.1$), asparagine, aspartate, glutamate, and glutamine showed a significant decrease due to *SNRK* knockdown ($p < 0.05$). This indicates significant changes in amino acid-related metabolic pathways, which is also observed in pathways analysis (Fig. 2C). Interestingly, glycerol was significantly increased due to *SNRK* knockdown relative to control (Fold Change: 1.38, $p = 0.018$). Glycerol can serve as substrate for energy in cardiomyocyte¹⁶ and we observe several other metabolites associated with energy metabolism including citrate, fumarate, malate, succinate ($p < 0.05$), pyruvate and NAD ($p < 0.1$) to be significantly reduced due to *SNRK* knockdown in CMs. This indicates that SNRK can play a crucial role in energy homeostasis in CMs.



Further pathway topology analysis (Fig. 2C) and metabolite set enrichment analysis (Fig. 2D) suggested significant changes in alanine, aspartate and glutamate metabolism ($p = 0.002$) (Fig. 2C and S2), citrate cycle ($p = 3.47E-06$) (Fig. 2C and S3), taurine and hypotaurine metabolism ($p = 0.002$), aminoacyl t-RNA biosynthesis ($p = 0.009$) and glycine, serine and threonine metabolism ($p = 0.01$) (Fig. 2C). Specific metabolites and amounts that changed in *SNRK* knockdown CMs are indicated in supplemental Tables S2 and S3. Taking the *in vivo* and *in vitro* data together, SNRK in CMs plays an instrumental role in maintaining metabolic homeostasis, which is critical for the normal functioning of the heart.

ROCK is a putative substrate of SNRK

To identify signaling proteins responsible for the cardiac function deficits observed in *Snrk* cmcKO mice *in vivo*, we performed a phosphopeptide proteomic screen using pure SNRK protein generated in the lab. Human histidine tagged SNRK protein was generated in bacteria (Fig. S4), purified (Fig. S4A), and confirmed by mass spectral (MS) analysis (23% peptide

coverage) and western blotted for SNRK antibody (Fig. S4D). Using this purified SNRK protein (Fig. S4E), we outsourced the kinase profiling to Life Technologies. An *in vitro* protein kinase experiment was performed on 9,000 N-terminal GST fusion proteins on an array at two SNRK protein concentrations (5 and 50 nM). This screen identified Rho-associated kinase 1 (ROCK1) as one of the top hits along with several members of the transforming growth factor- β (TGF- β) signaling pathway (ACVR1, ACVRL1, SMAD3, BMPR2) that showed 2-fold or more phosphorylation compared to negative control (Table. S4). We confirmed the ROCK1 phosphorylation *in vitro* using a ROCK kinase assay (Fig. 3A). ROCK1 protein was immunoprecipitated (IPed) from human umbilical vein endothelial cells (HUVECs) (Fig. 3A, IP blot), and was incubated with purified SNRK protein in the presence of radiolabeled phosphate (P^{32}). As shown (Fig. 3A, lane 2), a P^{32} -labeled band is observed in the lane with IPed ROCK plus SNRK protein at the correct size for the ROCK1 protein, which was quantified in three independent experiments (Fig. 3A, Quantitation panel). In addition, we performed multi-stage fragmentation tandem Mass Spectrometry on ROCK1 IPed from HUVECs in the presence or absence of SNRK. The ROCK1 band was excised and subjected to in-gel tryptic digestion. The resulting peptides were analyzed by multi-stage fragmentation mass spectral analysis¹⁷. The data for ROCK1 identified residues S27, T237, S479 (Fig. S5, blue circles) that resides in the N-terminal region. These sites are distinct from those reported in the literature (Fig. S5 magenta circles) or previously identified using proteomic approaches (Fig. S5, yellow highlighted residues). Collectively, this data suggests that ROCK1 is a direct target of SNRK, and phosphorylation of ROCK by SNRK at specific residues is likely to influence its downstream activity.

We next evaluated ROCK activity by determining the amount of phospho-Threonine 853

in the myosin-binding subunit (pMBS) of myosin light chain phosphatase, a key enzyme in the RhoA-ROCK muscle contraction signaling cycle. We performed western blots for ROCK1, ROCK2 and pMBS protein levels in *Snrk* cmcKO adult (Fig. 3B) heart lysates. Of the proteins investigated, pMBS levels were higher in adult *Snrk* cmcKO hearts (MYH6CRE SNRK L/L) (Fig. 3B, $p=0.1$) compared to CRE negative controls. We also investigated SNRK knockdown CMs *in vitro* for pMBS, and observed an increase that was not significant (Fig. 4A, $p=0.36$, $n=3$). Interestingly, when control and shSNRK knockdown CMs were treated with the ROCK inhibitor Y27632 (Fig. 4A), there was a slightly significant decrease in pMBS levels compared to control treated shSNRK knockdown CMs (40.75% $p=0.041$, $n=3$). Specific sample data values are indicated in supplemental Tables S1. Collectively, the phosphoproteomic analysis and signaling data suggests that ROCK is a substrate of SNRK, and ROCK activity is attenuated by SNRK *in vivo* and *in vitro* in CMs.

SNRK-ROCK signaling in cardiomyocytes

We next investigated signaling pathways that can be regulated by ROCK signaling such as protein kinase b alpha (AKT) and mitogen-activated protein kinase (ERK) in both *in vivo Snrk* cmcKO mice (Fig. 3B), and *in vitro* SNRK knockdown CMs (Fig. 4B-D). ROCK is known to regulate the phosphoinositide 3-kinase (PI3K)-AKT pathway by activating the phosphatidylinositol (3,4,5)-trisphosphate (PIP3) phosphatase called phosphatase and tensin homolog (PTEN), which results in a reduction in pAKT levels^{18, 19}. In addition, ROCK has also been shown to influence ERK signaling in smooth muscle cells²⁰. Western blot analysis was conducted on *Snrk* WT and cmcKO hearts lysates as well as control and shSNRK knockdown cells with and without the ROCK inhibitor Y27632. Loss of SNRK in the heart resulted in decreased pAKT (Fig. 3B, 46.15%, $p=0.1$, $n=3$) and the AKT downstream effector pIKK (Fig.

3B, 44.62%, $p=0.1$, $n=3$), which suggests decreased AKT signaling in the *Snrk* cmcKO hearts. We also observed a trend towards increased pERK (Fig. 3B, 183.47%, $p=0.2$, $n=3$) in the heart lysates. Specific sample data values are indicated in supplemental Tables S1.

Surprisingly knockdown of SNRK in CMs resulted in a non-significant change in pAKT (Fig. 4B, 171.07%, $p=0.136$, $n=4$) and pERK (Fig. 4D, 311.64%, $p=0.212$), and a significant increase in pIKK (Fig. 4C, 254.38%, $p=0.012$, $n=3$). Inhibition of ROCK signaling using the ROCK inhibitor Y27632 was able to significantly decrease the pMBS levels in the shSNRK CM compared to the control treated shSNRK CM (Fig. 4A, Control 123.35%, shSNRK 40.75% $p=0.041$, $n=3$). pAKT, pERK and pIKK levels did not significantly change in the presence of the ROCK inhibitor (Fig. 4C) suggesting that ROCK signaling is not the only molecule involved in regulating pAKT, pERK and pIKK signaling in cultured CMs. These results collectively suggest that SNRK directly influences ROCK signaling in CMs *in vivo* and *in vitro*.

SNRK-ROCK signaling is required for normal cardiac function

Altered ROCK signaling has been previously implicated cardiac hypertrophy and ventricular remodeling^{4, 21, 22}. To determine whether the cardiac defects observed in the *Snrk* cmcKO mice are attributed to increased ROCK activation, *Snrk* WT and *Snrk* cmcKO mice were treated with the ROCK inhibitor fasudil²³. To assess changes in cardiac function, ECHO was conducted before drug treatment and after 4 weeks of daily fasudil or saline injection (Fig. 5 and Table S5). Fasudil treatment in *Snrk* cmcKO mice resulted in stabilization of EF and FS phenotypes, from 55.55% (cmcKO-Fasudil) and 50.66% (cmcKO-Saline) EF and 24.77%-22.7% FS before treatment to 53% EF and 23.23% FS after fasudil treatment compared to the saline treated *Snrk* cmcKO mice which displayed continued declines in EF (44.55% $p=0.0286$) and FS (18.9% $p=0.0286$). EDV did not show a significant change in the *Snrk* cmcKO mice (0.0064) treated

with fasudil compared to baseline (0.0070, $p=0.6905$) whereas EDV continued to increase in the saline treated *Snrk* cmcKO mice from 0.0066 at baseline to 0.0082 at 4 week ($p=0.0286$). ESV did not increase in the fasudil treated *Snrk* cmcKO mice but did in the saline treated mice (baseline 0.0029 to 4 weeks 0.0046, $p=0.0286$) indicating a preserved EF in the fasudil treated mice. IVRT showed a similar trend with a slight decrease in the fasudil treated *Snrk* cmcKO mice (baseline 14.45 to 4 weeks 12.41, $p=0.3413$), and an increase in *Snrk* cmcKO saline treated mice (baseline 12.4 to 4 weeks 13.22, $p=0.0286$). These data indicates that increased ROCK activity is involved in generating the cardiac functional deficits observed in the *Snrk* cmcKO mice and that inhibition of ROCK results in cardiac functional improvements.

Discussion

In this study, we have identified that a member of the AMPK family namely SNRK influences ROCK signaling to maintain cardiac function in the adult. *Snrk* was first identified in 3T3-L1 differentiated adipocyte cells²⁴, and compared to *Ampkα1* and *Ampkα2*, *Snrk* expression in white adipose tissue, brown adipose tissue, heart and brain is significantly higher²⁵. The expression profile of SNRK, and the family that it belongs to suggest a role for this enzyme during high metabolic needs like the heart contraction and relaxation cycles. Indeed in our previous report⁷, we identified that SNRK is a critical regulator of metabolic function during embryonic cardiovascular development, and identified the metabolic pAMPK-pACC signaling pathway deregulation in the heart. These results directly support current NMR-based metabolomic analysis data in *SNRK* knockdown CMs, which shows decreased metabolites such as those involved in alanine, aspartate and glutamate metabolism (Fig. S2), as well as citric acid cycle metabolism (Fig. S3), and increases in metabolites involved in lipid synthesis such as glycerol (Fig S1)²⁶ which are processes directly influenced by pAMPK-pACC signaling^{27, 28}. Interestingly



perturbations in cardiac metabolic output have been observed in patients with heart failure^{29, 30}. In normal hearts, the primary metabolic energy source is derived by lipid metabolism/fatty acid oxidation and in failing hearts the metabolic substrate changes to glucose metabolism³¹. Furthermore, accumulation of lipids (free fatty acids) in the failing heart can create additional metabolic stress by increasing energy uncoupling and proton leakage and decreasing energy production^{32, 33}. In the *SNRK* knockdown CMs, we did not observe any significant changes in glycolysis or glucose metabolism but we did observe significant alterations in oxidative phosphorylation and lipid metabolism indicating an important role for SNRK in cardiac metabolism and loss of SNRK can result in a phenotypes similar to those observed during cardiac failure. In addition, taurine and hypotaurine metabolism was found to be increased in the *Snrk* knockdown CMs indicating the activation of compensatory mechanisms to increased osmotic stress^{34, 35}, and further supporting the notion that SNRK is an important regulator of cardiac cellular homeostasis.

To assess the contribution of SNRK to cardiac function, we conditionally deleted *Snrk* in CMs *in vivo* using MYH6CRE¹⁴ mouse line. The *Snrk* cmcKO mice develop cardiomyopathy and die at 8-10 months of age⁷. The 6 months ECHO studies showed changes in left ventricular dimensions and decreased ventricular function consistent with a dilated cardiomyopathy. Left heart failure often result in increased pulmonary artery pressures and our ECHO-Doppler interrogation of right heart hemodynamics corroborate this relationship. These mice over time progressively show increased fibrosis and cardiac stiffening, phenotypes associated with dysregulated ROCK signaling^{36, 37}. Indeed, we identified two key molecules namely the TGF- β signaling pathway and ROCK signaling pathways in our SNRK substrate screen both of which have been implicated in cardiac stiffening and fibrosis³⁷. We posit that SNRK's involvement in

the two signaling pathways may not be mutually exclusive since both have been implicated in CMs function previously. For example, TGF- β 3 and ALK2 regulate ROCK1 expression during valvuloseptal endocardial cushion formation³⁸, and up regulation of bone morphogenetic protein-2 (BMP-2), antagonized TGF- β 1/ROCK-enhanced cardiac fibrotic signal through activation of Smurf1/Smad6 complex³⁷. In this study, we only focused on ROCK because of the overwhelming evidence suggesting ROCK as a cardiovascular risk factor³⁹, and its role in cardiovascular physiology and pathophysiology⁴.

ROCKs' are ubiquitously expressed proteins, and both isoforms ROCK1 and ROCK2 are expressed in the heart⁴⁰. Signaling mechanisms associated with contraction in the vascular smooth muscle cells (SMCs) in the heart are well studied for ROCK. Briefly, intracellular Ca²⁺ level increases through activated G-protein coupled receptors, which in turn stimulate downstream phosphorylation of myosin light chain kinase (MLCK) (activating), and phosphorylation of the myosin binding subunit (MBS also known as MYPT1) of myosin light chain phosphatase (MLCP) (inactivating). The exchange factor RhoA is the chief upstream activator of ROCK1 to date, and has been the established regulator of this pathway⁴, the net result of which is contraction of SMCs. Our studies suggest SNRK is a second player upstream of ROCK but whether the phosphorylation directly activates or inhibits ROCK activity or whether additional proteins along with SNRK are required for altered ROCK activity is currently unknown. Our data suggests that SNRK is a negative regulator of ROCK signaling, and loss of SNRK increases ROCK activity in CMs. Indeed loss of SNRK in *Snrk* cmcKO adult (6 months) mice showed higher levels of pMBS reinforcing the hypothesis that phosphorylation of ROCK1 by SNRK may be inhibitory (Fig. 3). The converse experiment would be the overexpression or gain of SNRK in cardiac tissue, which should decrease ROCK activity and consequences

associated with it. The resulting phenotype would include improved cardiac function since ROCK1 is necessary for the transition from cardiac hypertrophy to failure⁴¹. Indeed two abstracts report that SNRK overexpression in the heart improves cardiac metabolic efficiency and response to myocardial ischemia^{42, 43}, which support our predictive hypothesis.

We also examined the activation status of additional downstream effectors of ROCK such as AKT and ERK and identified altered *in vivo* expression levels of pAKT and pERK further suggesting that ROCK activity are altered *in vivo* when SNRK is absent (Figs. 3 and 6).

Interestingly, we did not see a significant difference in the *in vitro* expression levels of pAKT, pERK and pMBS in *SNRK* knockdown CMs. These observations could be attributed to the inherent differences between *in vitro* culturing conditions and *in vivo* responses that contain additional non-CM cell types influencing the experimental readout. Additional *in vitro* studies are necessary to specifically address these differences.

To assess whether attenuation of ROCK signaling in *Snrk* cmcKO mice is consequential, we treated *Snrk* cmcKO mice with the ROCK inhibitor fasudil²³. Prior to treatment, the *Snrk* cmcKO already displayed cardiac functional defects. After 4 weeks of treatment with the inhibitor the *Snrk* cmcKO mice began showing signs of improved cardiac function and stabilization of the phenotype compared to the untreated *Snrk* cmcKO mice that continued to show decreased cardiac function (Fig. 5 and Table S5). These findings suggest that some of the cardiac functional deficits observed in the *Snrk* cmcKO mice are most likely a result increased ROCK activity and that SNRK regulation of ROCK signaling in an important component of normal cardiac function.

In summary, our data suggests that an AMPK family member SNRK is a critical metabolic sensor in cardiac tissues, and directly influences ROCK signaling in CMs, effects that

directly contribute to maintaining cardiac metabolic homeostasis and cardiac functional output in mammals.

Acknowledgments: We thank members of the Developmental Vascular Biology Program for their invaluable input and insight during the course of this study. We also thank Dmitry L. Sonin for assistance with the initiation of the mouse ECHO studies and the Children's Research Institute imaging core facilities for Hamamatsu slide scanner and visiopharm image analysis support and the Histology core for slide preparations. This publication was supported by the National Center for Advancing Translational Sciences, National Institutes of Health, through Grant Number UL1TR001436. Its contents are solely the responsibility of the authors and do not necessarily represent the official views of the NIH.

Sources of Funding: S.M.C., S.P., A.G., M.B., and R.R. are supported in part by funds from NIH grants HL102745 and HL112639, and Women's Health Research Program at MCW. J.S is supported by NIH grant HL111148 and S.P., V.J.B. and X.B. are supported by NIH grant EB007534. This publication was also supported by the National Center for Advancing Translational Sciences, NIH grant UL1TR001436.

Disclosures: None

References:

1. Alfieri O, Mayosi BM, Park SJ, Sarrafzadegan N, Virmani R. Exploring unknowns in cardiology. *Nat Rev Cardiol*. 2014;11:664-670.
2. Wang F, Zhang D, Wan A, Rodrigues B. Endothelial cell regulation of cardiac metabolism following diabetes. *Cardiovasc Hematol Disord Drug Targets*. 2014;14:121-125.
3. Budzyn K, Marley PD, Sobey CG. Targeting rho and rho-kinase in the treatment of cardiovascular disease. *Trends Pharmacol Sci*. 2006;27:97-104.
4. Loirand G, Guerin P, Pacaud P. Rho kinases in cardiovascular physiology and pathophysiology. *Circ Res*. 2006;98:322-334.

5. Zhou H, Li YJ, Wang M, Zhang LH, Guo BY, Zhao ZS, et al. Involvement of rhoa/rock in myocardial fibrosis in a rat model of type 2 diabetes. *Acta Pharmacol Sin.* 2011;32:999-1008.
6. Chun CZ, Kaur S, Samant GV, Wang L, Pramanik K, Garnaas MK, et al. Snrk-1 is involved in multiple steps of angioblast development and acts via notch signaling pathway in artery-vein specification in vertebrates. *Blood.* 2009;113:1192-1199.
7. Cossette SM, Gastonguay AJ, Bao X, Lerch-Gaggl A, Zhong L, Harmann LM, et al. Sucrose non-fermenting related kinase enzyme is essential for cardiac metabolism. *Biol open.* 2014;BIO20149811.
8. Breckenridge RA, Piotrowska I, Ng KE, Ragan TJ, West JA, Kotecha S, et al. Hypoxic regulation of hand1 controls the fetal-neonatal switch in cardiac metabolism. *PLoS Biol.* 2013;11:e1001666.
9. Lopaschuk GD, Jaswal JS. Energy metabolic phenotype of the cardiomyocyte during development, differentiation, and postnatal maturation. *J Cardiovasc Pharmacol.* 2010;56:130-140.
10. Bhute VJ, Palecek SP. Metabolic responses induced by DNA damage and poly (adp-ribose) polymerase (parp) inhibition in mcf-7 cells. *Metabolomics.* 2015;11:1779-1791.
11. Weljie AM, Newton J, Mercier P, Carlson E, Slupsky CM. Targeted profiling: Quantitative analysis of 1h nmr metabolomics data. *Anal Chem.* 2006;78:4430-4442.
12. Wishart DS, Jewison T, Guo AC, Wilson M, Knox C, Liu Y, et al. Hmdb 3.0--the human metabolome database in 2013. *Nucleic Acids Res.* 2013;41:D801-807.
13. Xia J, Sinelnikov IV, Han B, Wishart DS. Metaboanalyst 3.0--making metabolomics more meaningful. *Nucleic Acids Res.* 2015;43:W251-257.
14. Agah R, Frenkel PA, French BA, Michael LH, Overbeek PA, Schneider MD. Gene recombination in postmitotic cells. Targeted expression of cre recombinase provokes cardiac-restricted, site-specific rearrangement in adult ventricular muscle in vivo. *J Clin Invest.* 1997;100:169-179.
15. Kim S, Iwao H. Molecular and cellular mechanisms of angiotensin ii-mediated cardiovascular and renal diseases. *Pharmacol Rev.* 2000;52:11-34.
16. Hibuse T, Maeda N, Nakatsuji H, Tochino Y, Fujita K, Kihara S, et al. The heart requires glycerol as an energy substrate through aquaporin 7, a glycerol facilitator. *Cardiovasc Res.* 2009;83:34-41.
17. Narayan M, Mirza SP, Twining SS. Identification of phosphorylation sites on extracellular corneal epithelial cell maspin. *Proteomics.* 2011;11:1382-1390.

18. Yang S, Kim HM. The rhoa-rock-pten pathway as a molecular switch for anchorage dependent cell behavior. *Biomaterials*. 2012;33:2902-2915.
19. Chang J, Xie M, Shah VR, Schneider MD, Entman ML, Wei L, et al. Activation of rho-associated coiled-coil protein kinase 1 (rock-1) by caspase-3 cleavage plays an essential role in cardiac myocyte apoptosis. *Proc Natl Acad Sci U S A*. 2006;103:14495-14500.
20. Liu Y, Suzuki YJ, Day RM, Fanburg BL. Rho kinase-induced nuclear translocation of erk1/erk2 in smooth muscle cell mitogenesis caused by serotonin. *Circ Res*. 2004;95:579-586.
21. Kobayashi N, Horinaka S, Mita S, Nakano S, Honda T, Yoshida K, et al. Critical role of rho-kinase pathway for cardiac performance and remodeling in failing rat hearts. *Cardiovasc Res*. 2002;55:757-767.
22. Hattori T, Shimokawa H, Higashi M, Hiroki J, Mukai Y, Tsutsui H, et al. Long-term inhibition of rho-kinase suppresses left ventricular remodeling after myocardial infarction in mice. *Circulation*. 2004;109:2234-2239.
23. Shi J, Wei L. Rho kinases in cardiovascular physiology and pathophysiology: The effect of fasudil. *J Cardiovasc Pharmacol*. 2013;62:341-354.
24. Becker W, Heukelbach J, Kentrup H, Joost HG. Molecular cloning and characterization of a novel mammalian protein kinase harboring a homology domain that defines a subfamily of serine/threonine kinases. *Eur J Biochem*. 1996;235:736-743.
25. Guttman M, Russell P, Ingolia NT, Weissman JS, Lander ES. Ribosome profiling provides evidence that large noncoding rnas do not encode proteins. *Cell*. 2013;154:240-251.
26. D'Souza K, Nzirorera C, Kienesberger PC. Lipid metabolism and signaling in cardiac lipotoxicity. *Biochim Biophys Acta*. 2016.
27. Appuhamy JA, Nayananjalie WA, England EM, Gerrard DE, Akers RM, Hanigan MD. Effects of amp-activated protein kinase (ampk) signaling and essential amino acids on mammalian target of rapamycin (mTOR) signaling and protein synthesis rates in mammary cells. *J Dairy Sci*. 2014;97:419-429.
28. O'Neill HM, Holloway GP, Steinberg GR. Ampk regulation of fatty acid metabolism and mitochondrial biogenesis: Implications for obesity. *Mol Cell Endocrinol*. 2013;366:135-151.
29. Nagoshi T, Yoshimura M, Rosano GM, Lopaschuk GD, Mochizuki S. Optimization of cardiac metabolism in heart failure. *Curr Pharm Des*. 2011;17:3846-3853.
30. Stanley WC, Recchia FA, Lopaschuk GD. Myocardial substrate metabolism in the normal and failing heart. *Physiol Rev*. 2005;85:1093-1129.

31. Davila-Roman VG, Vedala G, Herrero P, de las Fuentes L, Rogers JG, Kelly DP, et al. Altered myocardial fatty acid and glucose metabolism in idiopathic dilated cardiomyopathy. *J Am Coll Cardiol.* 2002;40:271-277.
32. O'Donnell JM, Fields AD, Sorokina N, Lewandowski ED. The absence of endogenous lipid oxidation in early stage heart failure exposes limits in lipid storage and turnover. *J Mol Cell Cardiol.* 2008;44:315-322.
33. Boudina S, Sena S, O'Neill BT, Tathireddy P, Young ME, Abel ED. Reduced mitochondrial oxidative capacity and increased mitochondrial uncoupling impair myocardial energetics in obesity. *Circulation.* 2005;112:2686-2695.
34. Wang GG, Li W, Lu XH, Zhao X, Xu L. Taurine attenuates oxidative stress and alleviates cardiac failure in type i diabetic rats. *Croat Med J.* 2013;54:171-179.
35. Schaffer SW, Jong CJ, Ramila KC, Azuma J. Physiological roles of taurine in heart and muscle. *J Biomed Sci.* 2010;17 Suppl 1:S2.
36. Rikitake Y, Oyama N, Wang CY, Noma K, Satoh M, Kim HH, et al. Decreased perivascular fibrosis but not cardiac hypertrophy in rock1^{+/-} haploinsufficient mice. *Circulation.* 2005;112:2959-2965.
37. Wang S, Sun A, Li L, Zhao G, Jia J, Wang K, et al. Up-regulation of bmp-2 antagonizes tgfbeta1/rock-enhanced cardiac fibrotic signalling through activation of smurf1/smad6 complex. *J Cell Mol Med.* 2012;16:2301-2310.
38. Sakabe M, Sakata H, Matsui H, Ikeda K, Yamagishi T, Nakajima Y. Rock1 expression is regulated by tgfbeta3 and alk2 during valvuloseptal endocardial cushion formation. *Anat Rec.* 2008;291:845-857.
39. Soga J, Noma K, Hata T, Hidaka T, Fujii Y, Idei N, et al. Rho-associated kinase activity, endothelial function, and cardiovascular risk factors. *Arterioscler Thromb Vasc Biol.* 2011;31:2353-2359.
40. Zhao Z, Rivkees SA. Rho-associated kinases play a role in endocardial cell differentiation and migration. *Dev Biol.* 2004;275:183-191.
41. Shi J, Zhang YW, Yang Y, Zhang L, Wei L. Rock1 plays an essential role in the transition from cardiac hypertrophy to failure in mice. *J Mol Cell Cardiol.* 2010;49:819-828.
42. Rines AM, Wu R, Khechaduri A, Burke MA, Sato T, Abdelwahid E, et al. Abstract: Snf1-related kinase improves cardiac metabolic efficiency through a decrease in mitochondrial uncoupling. *Circulation.* 2014:A14048.

43. Rines A, Burke MA, Wu R, Abel DA, Ardehali H. Abstract: Transgenic overexpression of snf1-related kinase in the heart improves cardiac metabolic efficiency and response to myocardial ischemis. *Circ Res.* 2012:A11.

Figure Legends:

Figure 1: Cardiomyocyte-conditional SNRK null mice (*Snrk* cmcKO) ECHO results. ECHO was performed on 6 month adult *Snrk* WT and cmcKO males as described in the materials and methods. Panel A describes strain and strain rate imaging analyses by ECHO. Panel B indicates isovolumic relaxation time (IVRT) msec, a parameter for diastolic function, ratio of mitral peak velocity of early filling (E) m to early diastolic mitral annular velocity (e') (E/e' ratio), pulmonary acceleration time (PAT) msec, ejection time (ET) msec and ratio of PAT to ET. Panel C shows time-velocity integrals (TVI) cm along with mitral peak velocity (E) m/s and diastolic mitral annular velocity (e') m/s. Panel D are representative images of Gomori's Trichrome staining in CRE negative or cardiomyocyte specific conditional null (MYH6CRE SNRK L/L) adult mouse hearts. Panel E, shows average percent collagen staining in CRE negative MYH6CRE SNRK L/L adult mouse hearts. The number of mice per group equals 3-5. *= $p < 0.05$, #= $p < 0.1$. Scale bar = 1mm

Figure 2: Loss of SNRK results in altered metabolomic profiles. Panel A. Heat map depicting the altered identified metabolites in non-silencing shRNA control (CNT) and shSNRK

knockdown (SNRK) cardiomyocytes. Panel B Score Plot analysis for principle components (PC) between the non-silencing shRNA control (CNT) red and shSNRK knockdown (SNRK) green cardiomyocytes. Panel C Pathway topology analysis. Panel D. Metabolite set enrichment analysis was used to identify significantly enriched pathways ($p < 0.05$).

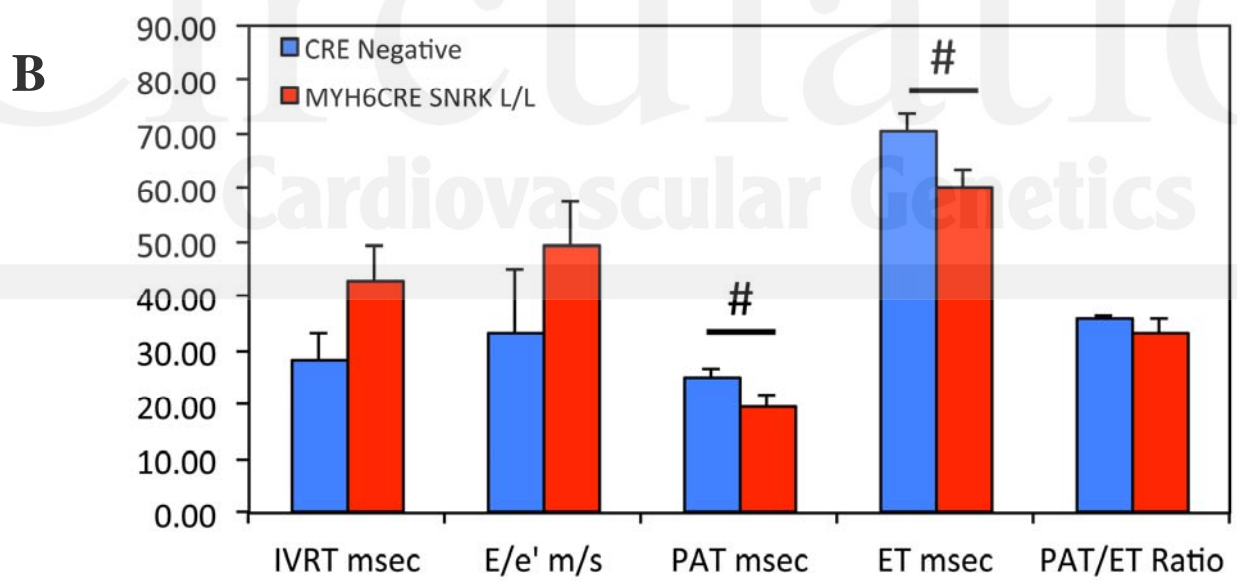
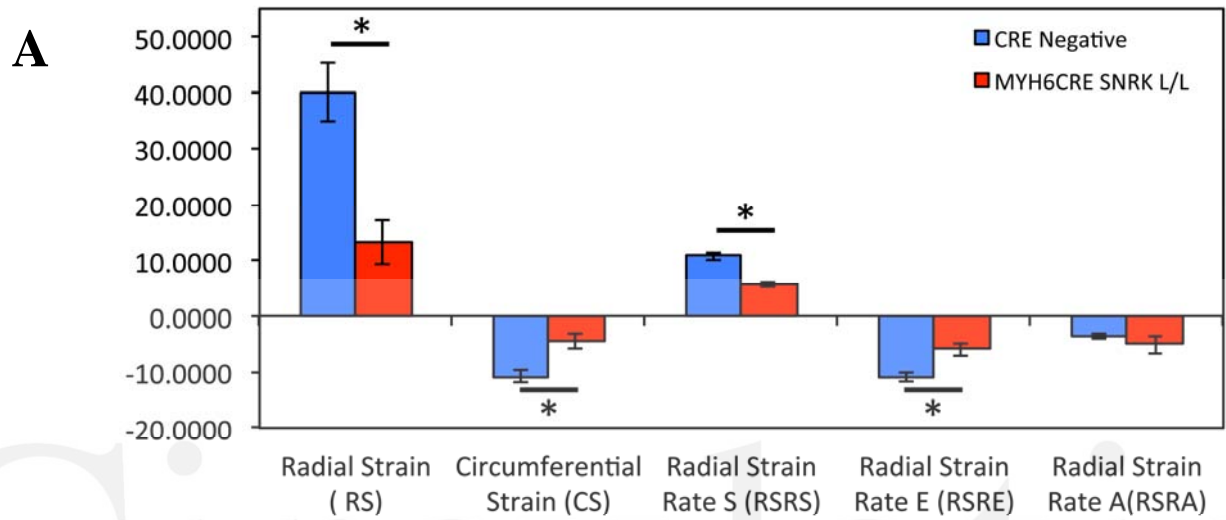
Figure 3: SNRK phosphorylation of ROCK, and influences on its activity in *Snrk* cmcKO adult hearts. Panel A shows direct phosphorylation of immunoprecipitated ROCK1 from human umbilical vein endothelial cells. Quantitation of the radioactive band in A is shown, and the successful immunoprecipitation of ROCK1 is demonstrated with the ROCK antibody on IPed lysates. Arrow denotes ROCK1 band. Data represents 3-4 independent experiments. Panel B western blot quantitation on lysates from cardiomyocyte-deleted SNRK adult hearts. Panel C representative western blot images from 4 independent heart lysates. The number of mice per group equals 3.

Figure 4: Loss of *Snrk* in cardiomyocytes results in increased ROCK activity. Western blots were performed on cardiomyocytes as described in materials and methods. Panel A-D western blot quantification of cardiomyocytes treated with water (Control), or 5 μ M ROCK Inhibitor Y27632. Data represents 3-4 independent experiments. $*=p < 0.05$, $**=p < 0.0125$.

Figure 5: Inhibition of ROCK signaling improved cardiac function in cardiomyocyte-conditional SNRK null mice (*Snrk* cmcKO). ECHO was performed on 6-4 month adult male and female *Snrk* WT and *Snrk* cmcKO mice immediately prior to treatment and after 4 weeks. The mice received daily injections of saline or fasudil as described in the materials and methods. Panel A

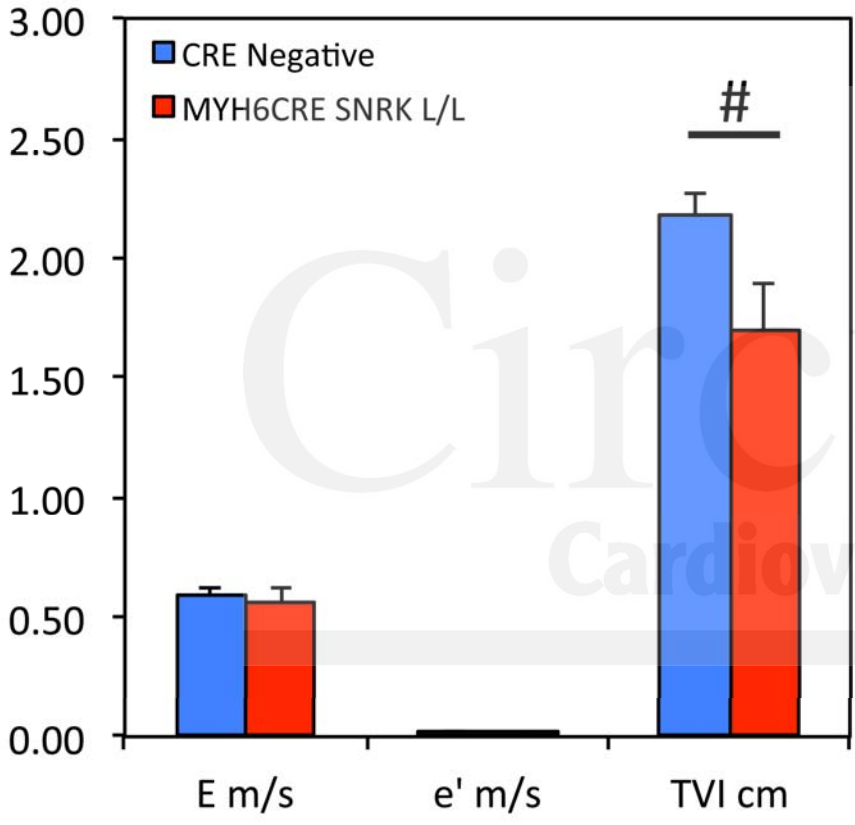
and B describes left ventricular (LV) function parameters EF % and FS %. Panel C and D describes the EDV and ESV which were normalized to body weight (BW). Panel E indicates the IVRT msec. Panel F is a representative M-Mode images from the mouse hearts at baseline or after 4 weeks of daily fasudil or saline injections. There were 2 males and 2 females in the saline treated *Snrk* cmcKO and *Snrk* WT groups and 2 males and 3 females in the fasudil treated *Snrk* cmcKO and *Snrk* WT groups. See Table S5 for complete data set.

Figure 6: Proposed model for the mechanism of SNRK regulation of ROCK activity. ROCK is a major downstream effector of the small GTPase RhoA. Upon activation, ROCK can influence cellular contraction by phosphorylating myosin-binding subunit (MBS, also known as MYPT-1) of the myosin phosphatase complex. Phosphorylation of the myosin phosphatase complex renders the complex inactive and it is no longer able to remove the active phosphate group from phosphorylated myosin light chain (pMLC). Phosphorylated MLC is active and able to promote cellular contraction. SNRK regulates this process by modulating ROCK activity via phosphorylation of ROCK. ROCK can also influence ERK phosphorylation and nuclear localization as well as activate PTEN, which in turns inhibits the PI3K pathway resulting in the inhibition of phospho-AKT.

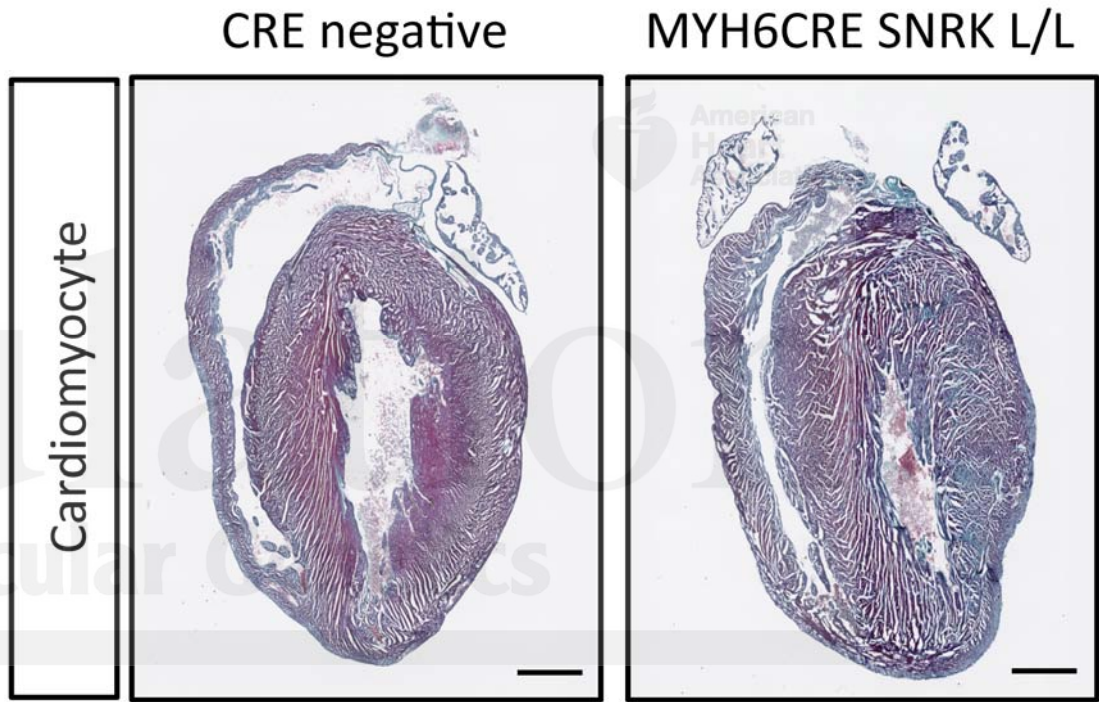


Circulation
Cardiovascular Genetics

C

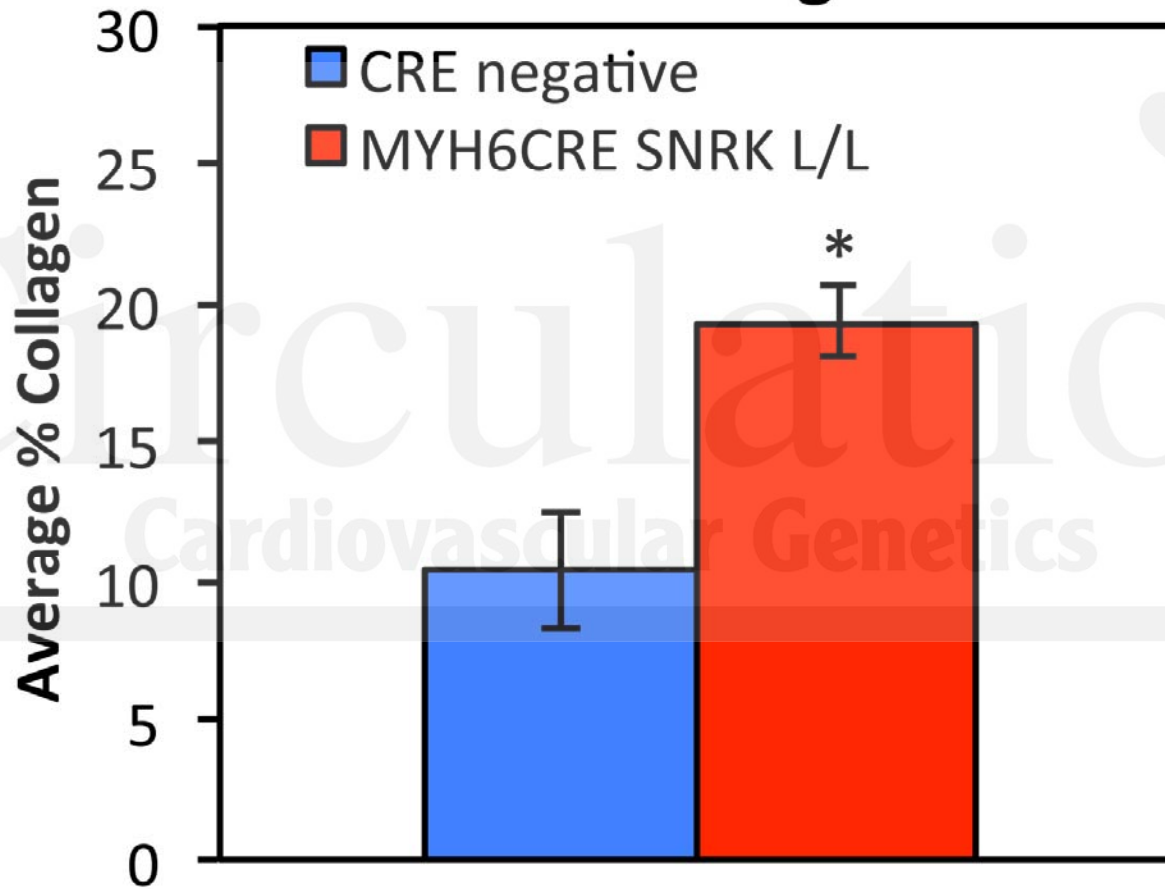


D

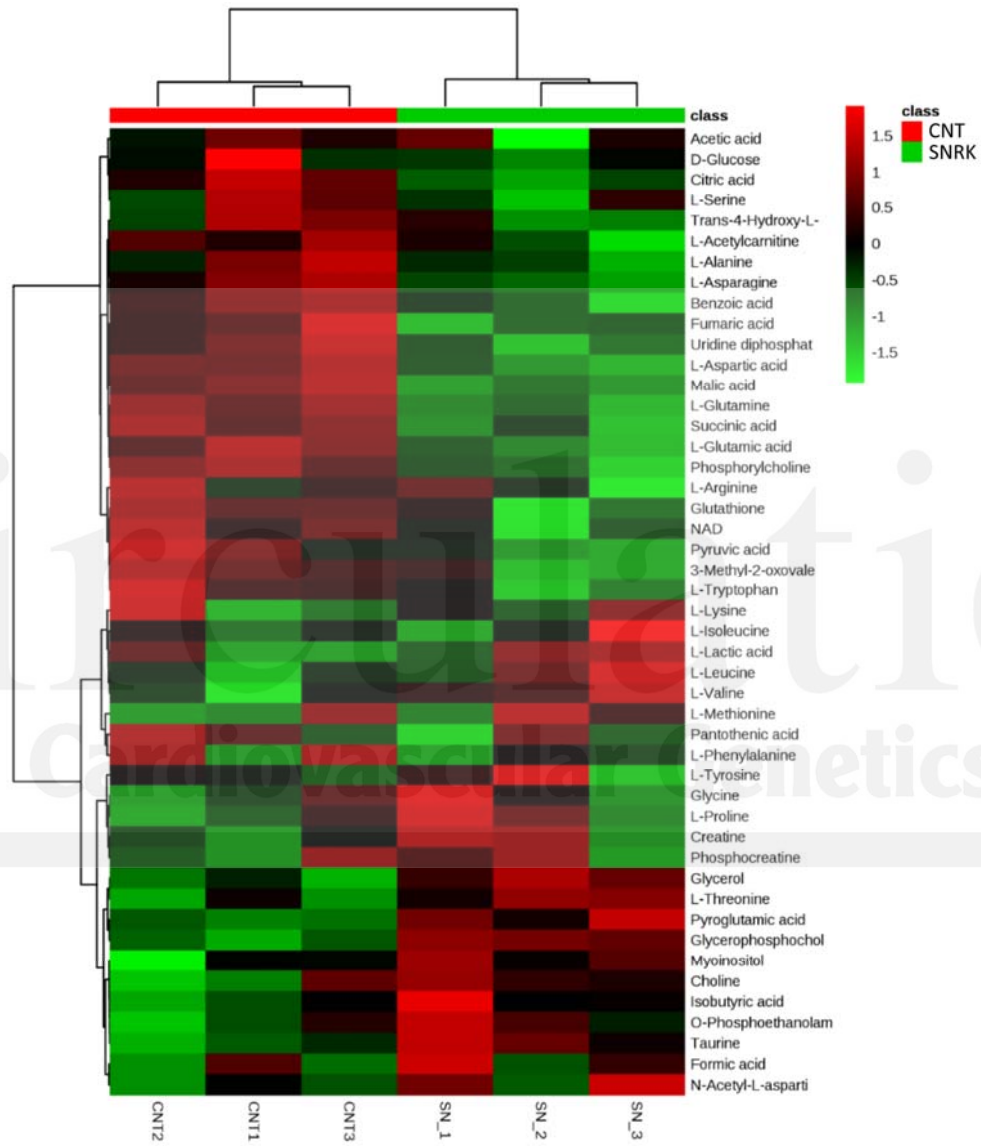


E

Quantification of Trichrome Staining



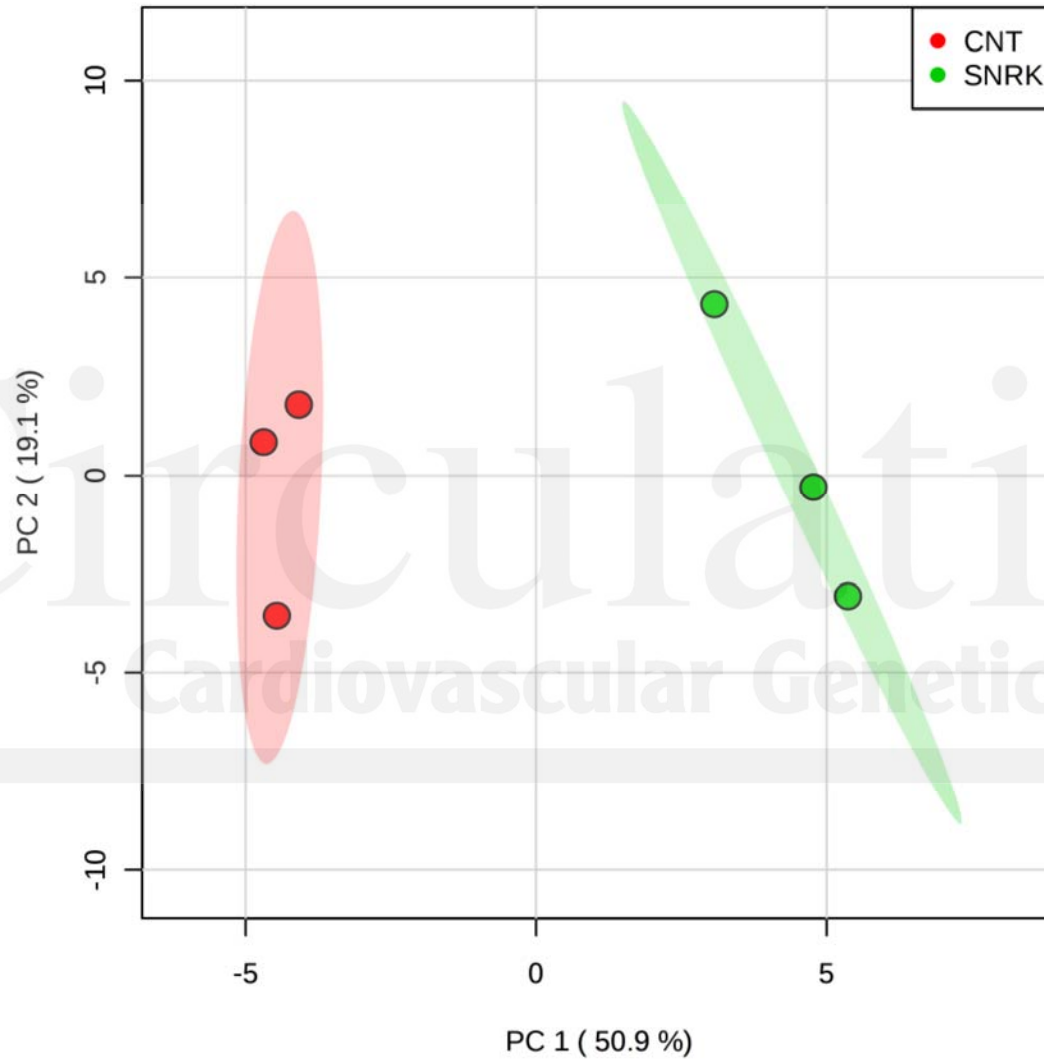
A



Circulation
Cardiovascular Genetics

B

Scores Plot

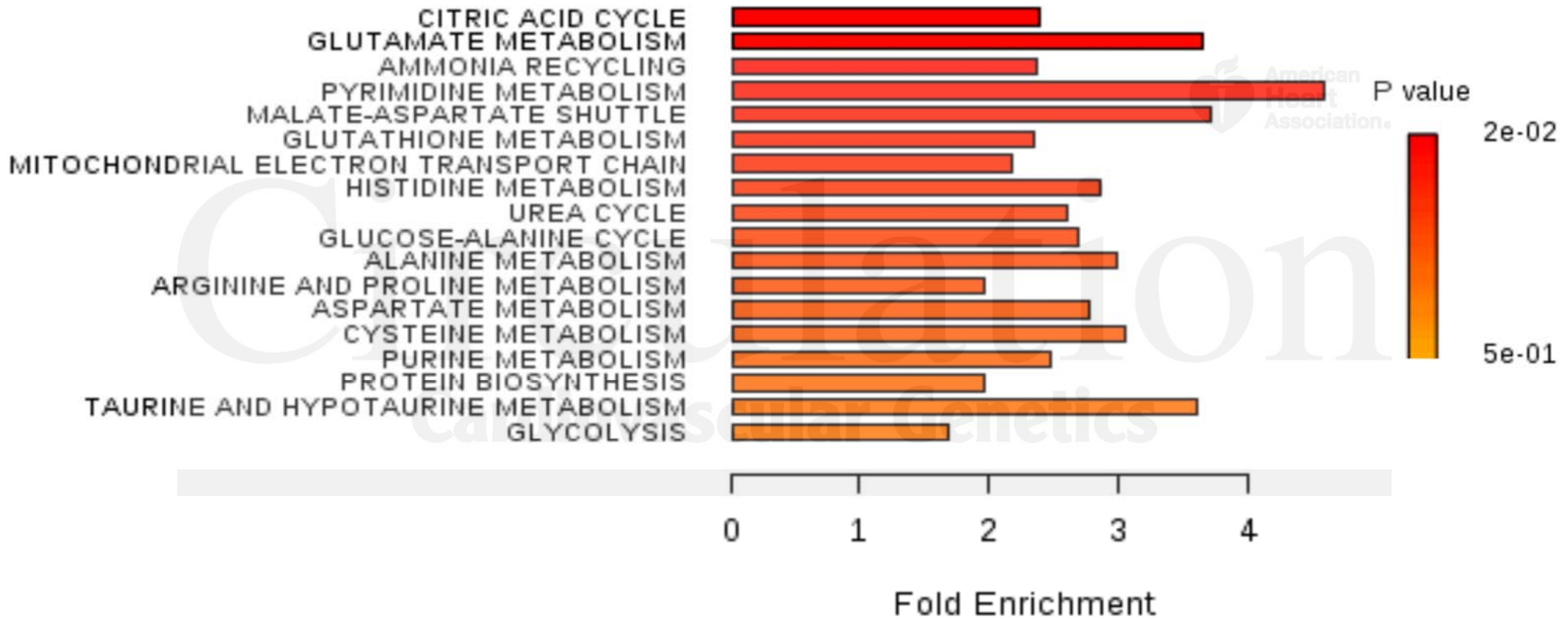


Circulation
Cardiovascular Genetics

C

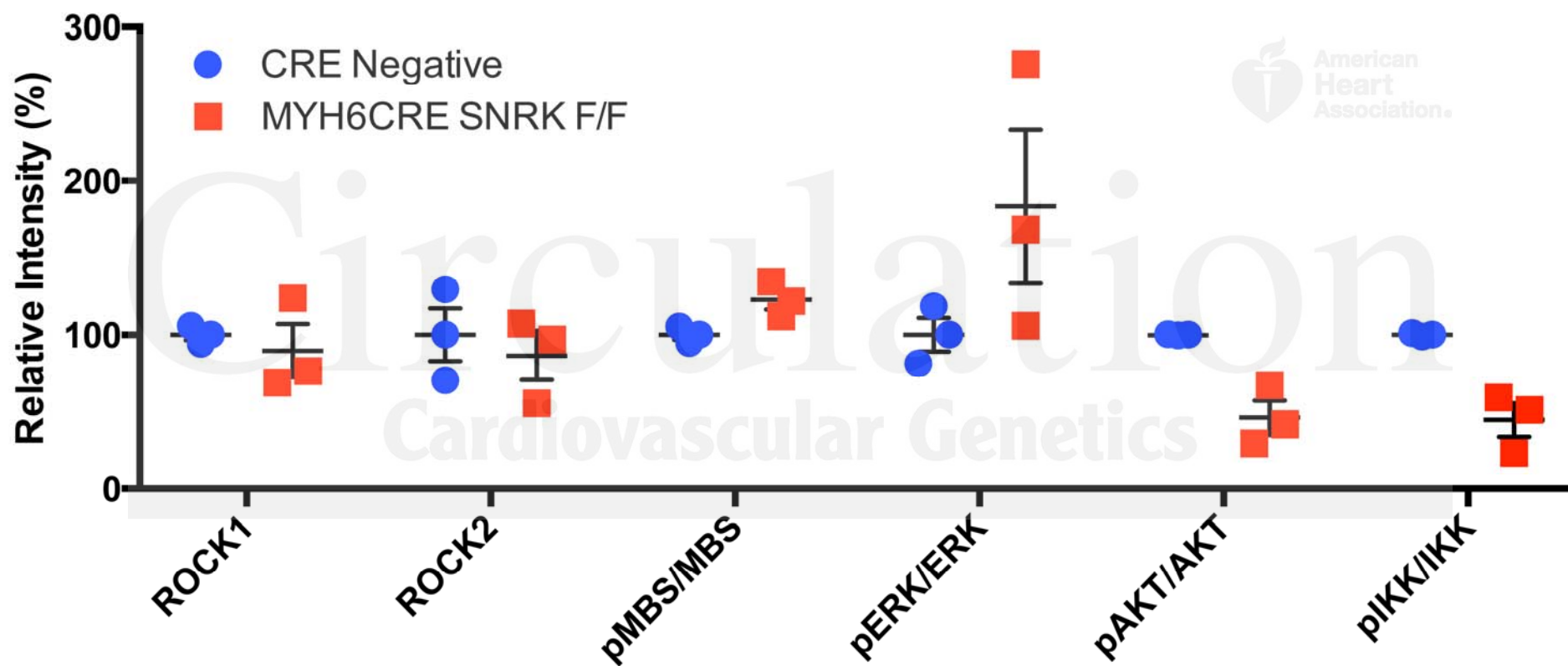
PATHWAY	Hits	Raw p	FDR	Impact
Citrate cycle (TCA cycle)	4	3.47E-06	0.000181	0.1875
Arginine and proline metabolism	10	0.000141	0.00359	0.26214
Nitrogen metabolism	10	0.000212	0.00359	0.26922
Tyrosine metabolism	4	0.000287	0.00359	0.07778
Butanoate metabolism	4	0.000345	0.00359	0.08
Glyoxylate and dicarboxylate metabolism	4	0.000985	0.007407	0.09091
Glutathione metabolism	4	0.000997	0.007407	0.17742
D-Glutamine and D-glutamate metabolism	2	0.001398	0.008076	0.33334
Nicotinate and nicotinamide metabolism	4	0.001857	0.009467	0.07273
Porphyrin and chlorophyll metabolism	3	0.002063	0.009467	0.02631
Pyrimidine metabolism	1	0.002441	0.009467	0.01031
Alanine, aspartate and glutamate metabolism	9	0.002597	0.009467	0.68571
Phenylalanine metabolism	6	0.002745	0.009467	0.16363
Taurine and hypotaurine metabolism	4	0.002913	0.009467	0.43479
Histidine metabolism	2	0.003549	0.010856	0.02
beta-Alanine metabolism	2	0.006719	0.019411	0.0303
Aminoacyl-tRNA biosynthesis	18	0.00907	0.024467	0.35486
Cyanoamino acid metabolism	4	0.00941	0.024467	0.24999
Glycine, serine and threonine metabolism	8	0.010867	0.026908	0.38983
Pantothenate and CoA biosynthesis	4	0.012511	0.029572	0.15151
Purine metabolism	2	0.015158	0.033194	0.00714
Glycerophospholipid metabolism	4	0.01532	0.033194	0.1233
Cysteine and methionine metabolism	6	0.016594	0.033931	0.09878
Glycerolipid metabolism	1	0.016965	0.033931	0.11111
Propanoate metabolism	3	0.026944	0.051893	0.06249
Amino sugar and nucleotide sugar metabolism	2	0.044392	0.082443	0.06422
Lysine biosynthesis	2	0.047813	0.085734	0.05714

D



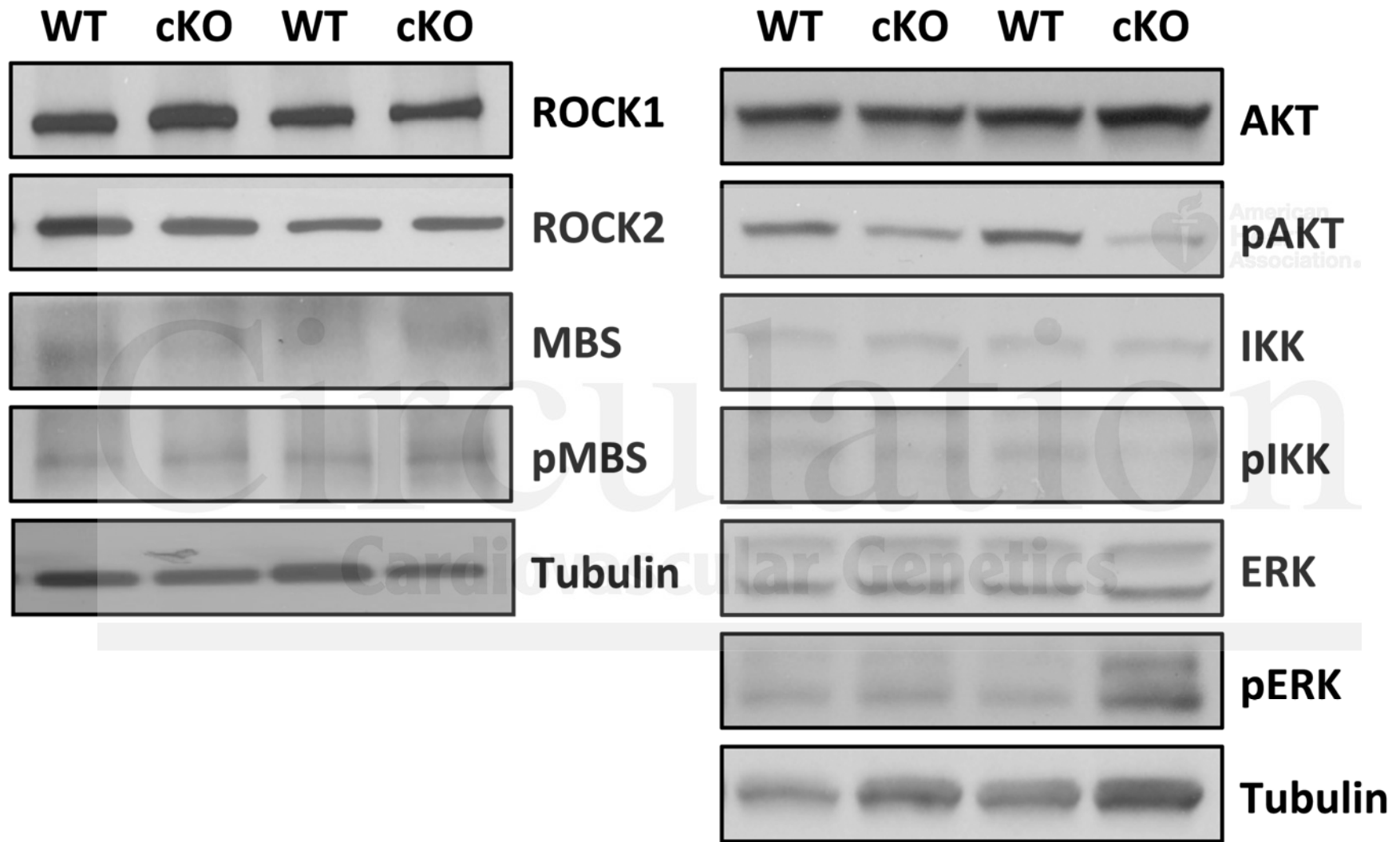
B

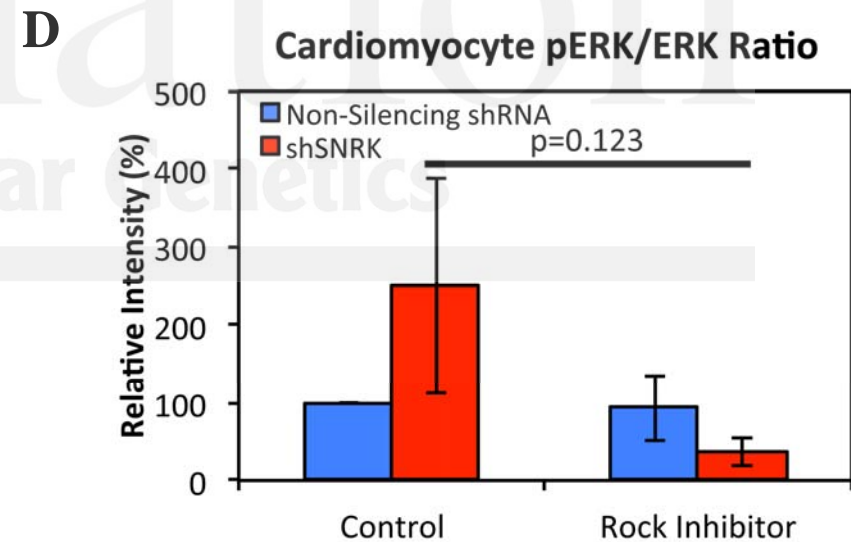
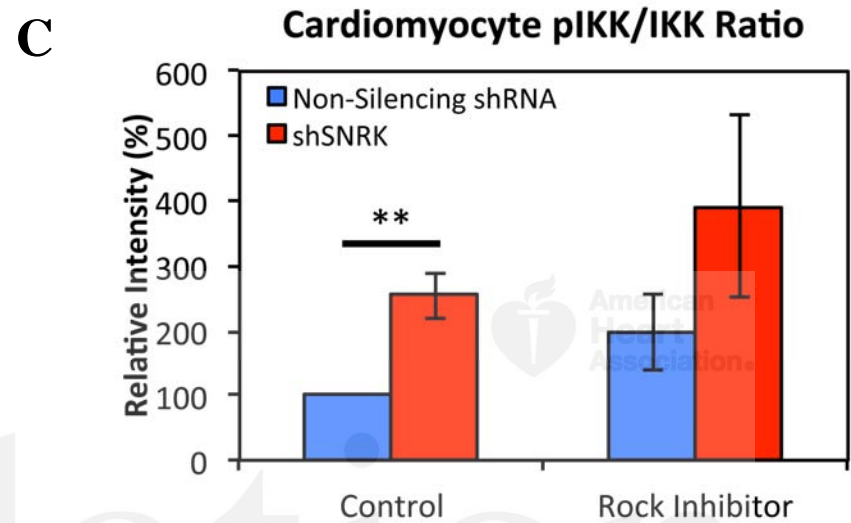
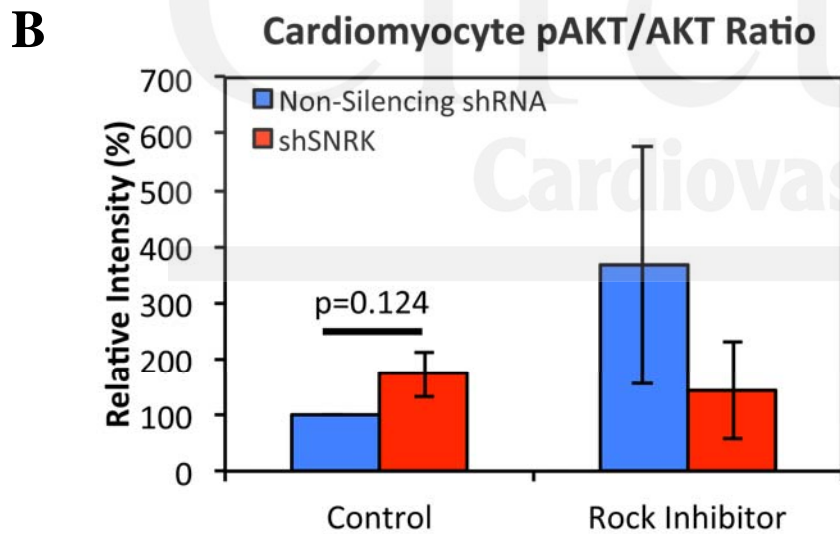
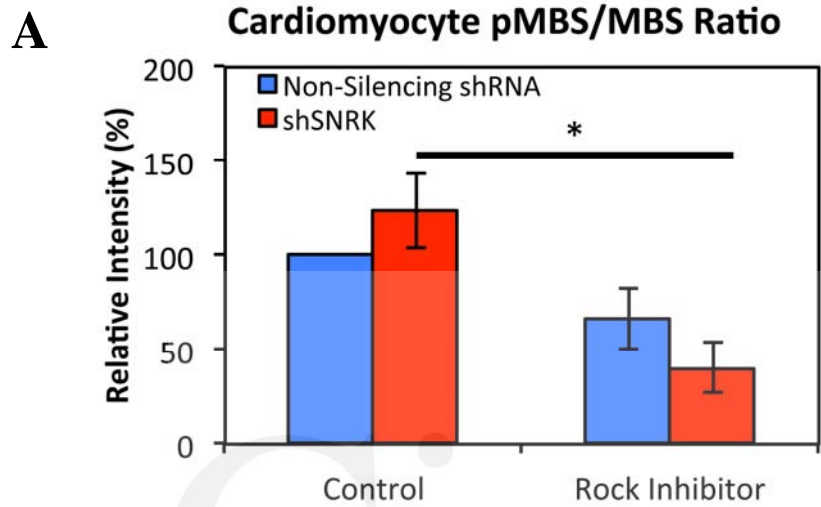
MYH6CRE Adult Heart Analysis

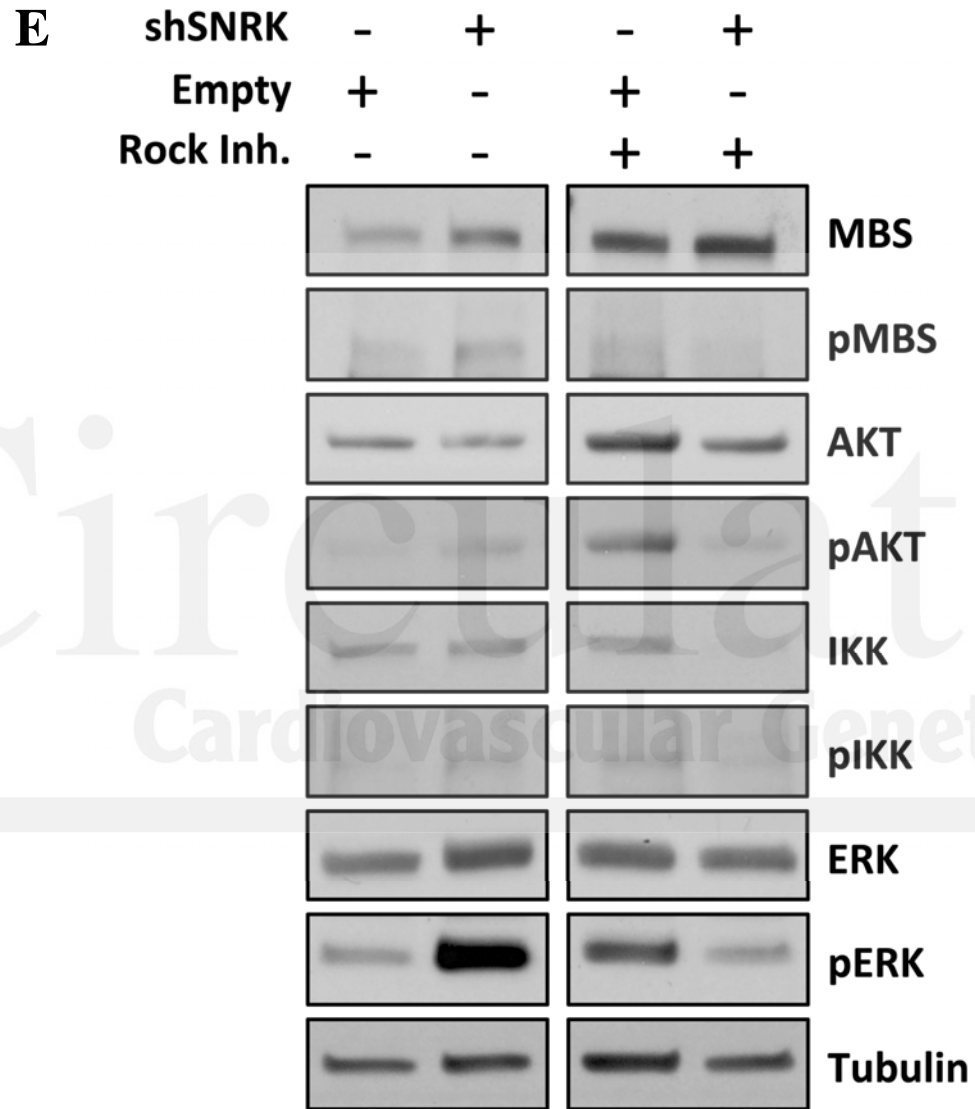


Circulation
Cardiovascular Genetics

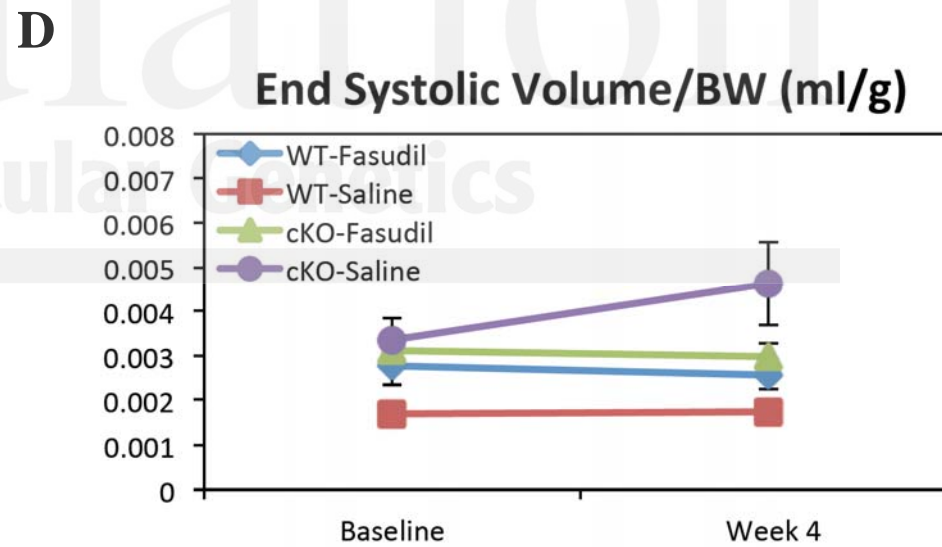
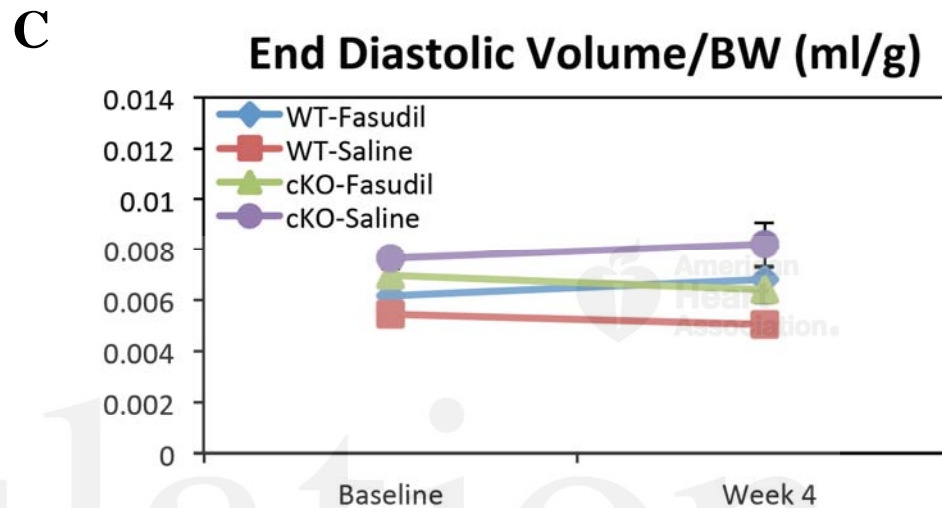
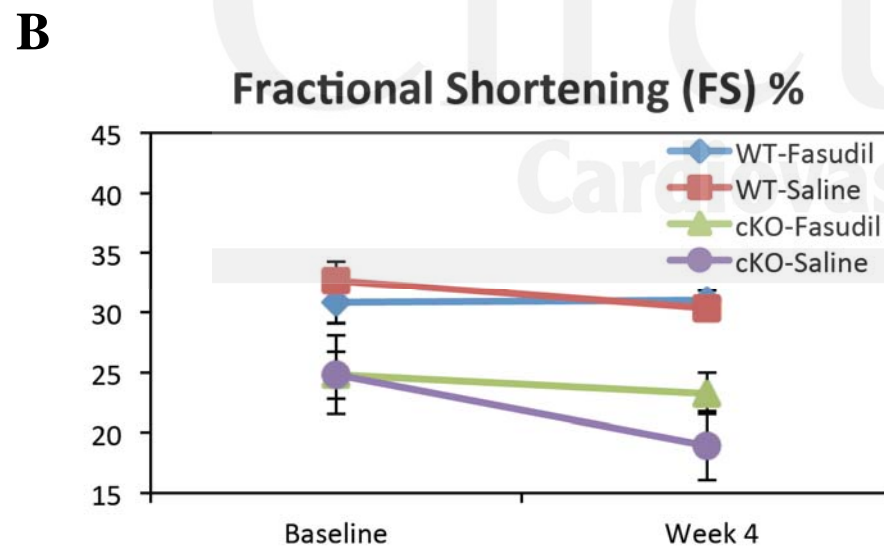
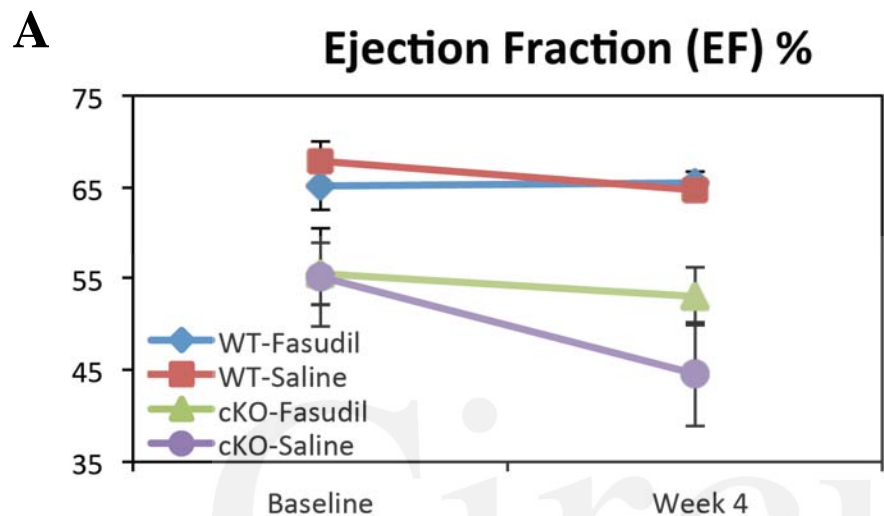
C



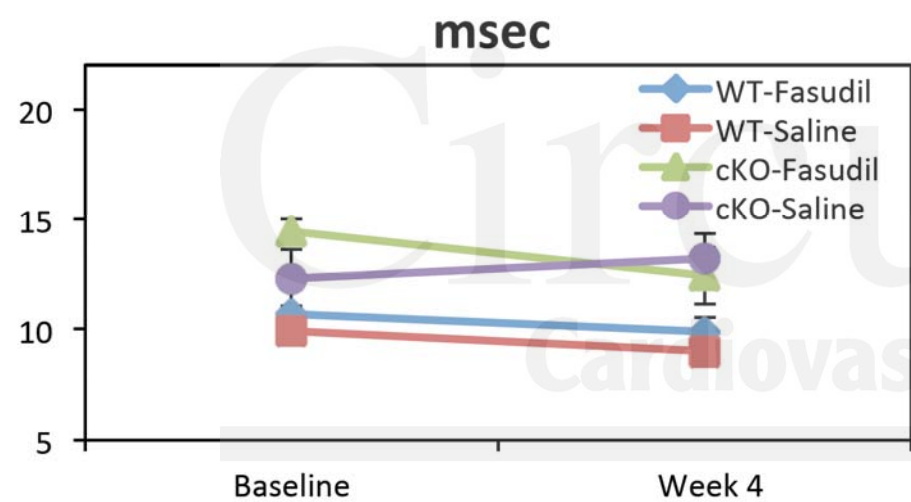




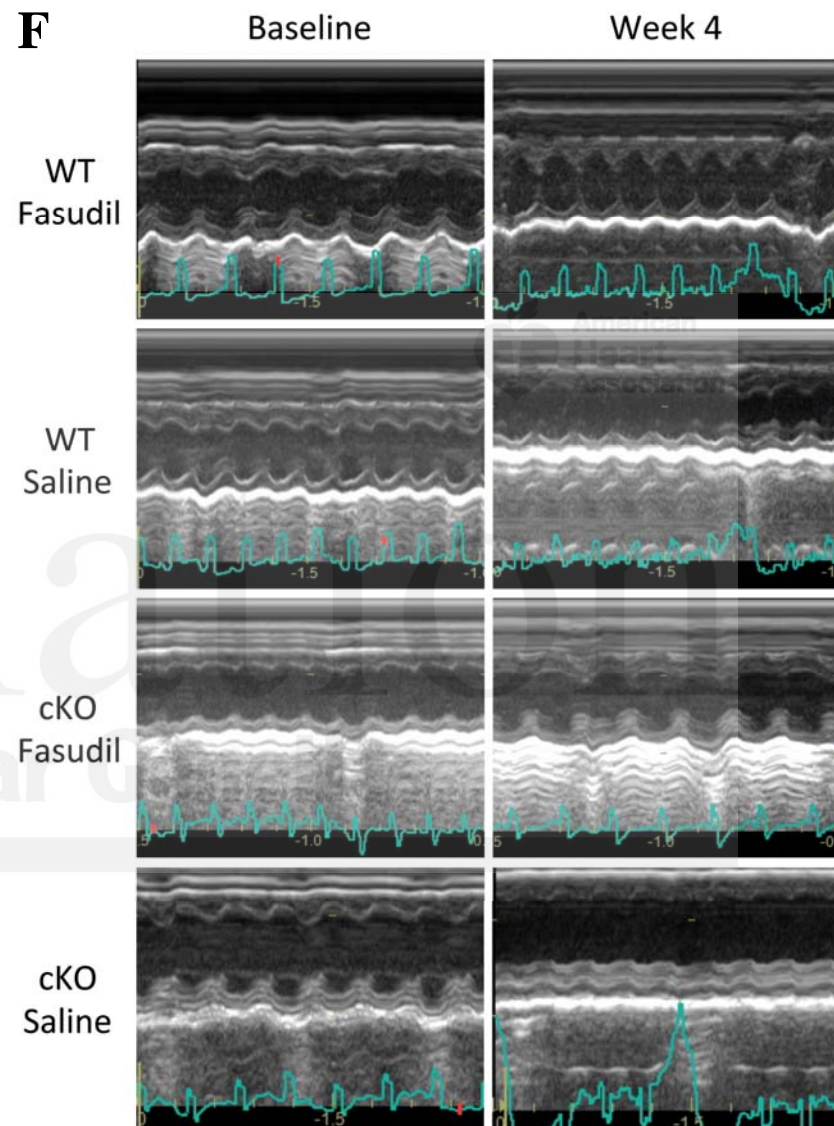
Circulation
Cardiovascular Genetics

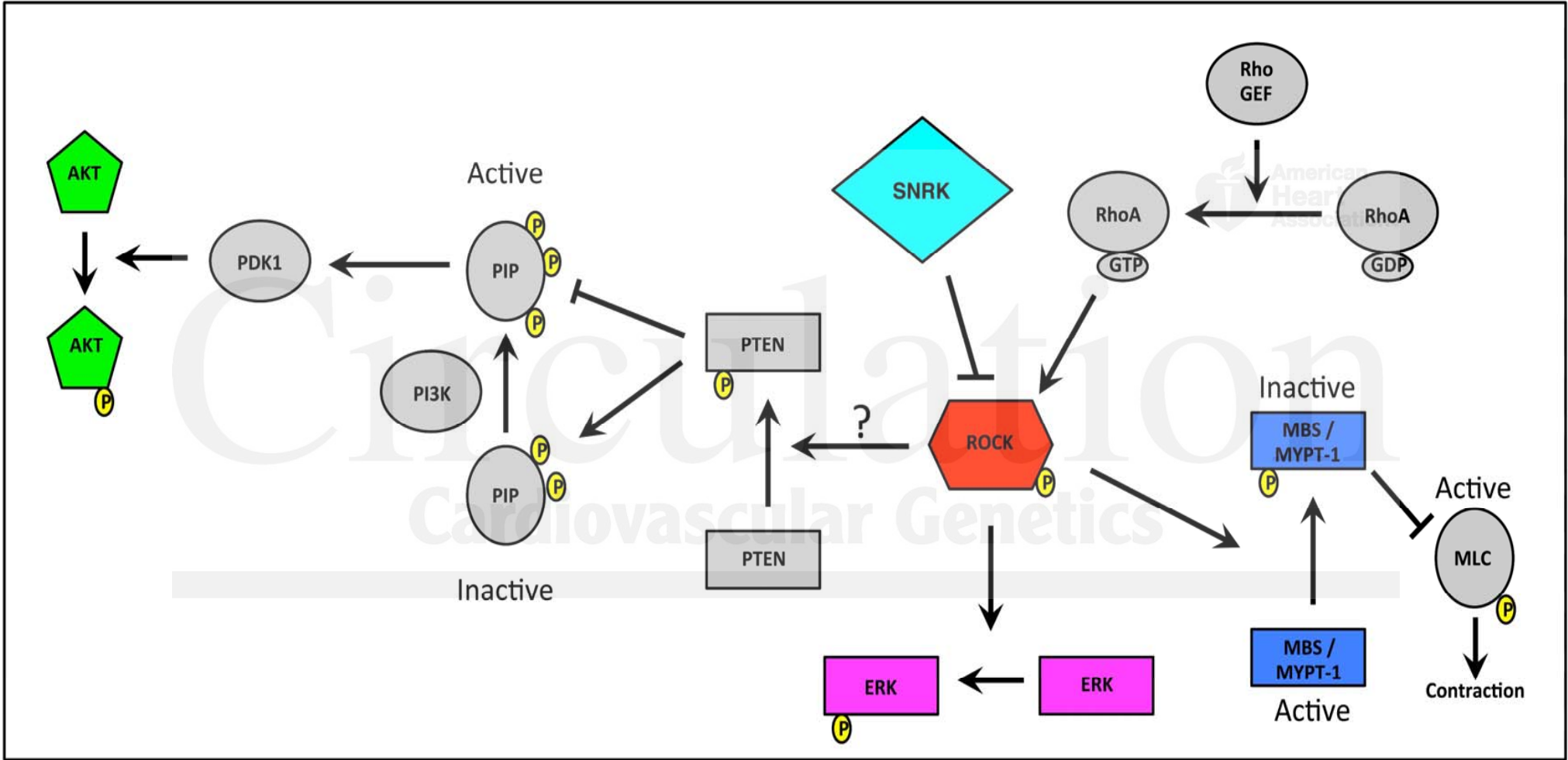


E Isovolumic relaxation time (IVRT)



F





Sucrose Non-Fermenting Related Kinase Enzyme Mediated Rho-Associated Kinase Signaling is Responsible for Cardiac Function

Stephanie M. Cossette, Vijesh J. Bhute, Xiaoping Bao, Leanne M. Harmann, Mark A. Horswill, Indranil Sinha, Adam Gastonguay, Shabnam Pooya, Michelle Bordas, Suresh N. Kumar, Shama P. Mirza, Sean Palecek, Jennifer Strande and Ramani Ramchandran

Circ Cardiovasc Genet. published online October 25, 2016;
Circulation: Cardiovascular Genetics is published by the American Heart Association, 7272 Greenville Avenue, Dallas, TX 75231
Copyright © 2016 American Heart Association, Inc. All rights reserved.
Print ISSN: 1942-325X. Online ISSN: 1942-3268

The online version of this article, along with updated information and services, is located on the World Wide Web at:

<http://circgenetics.ahajournals.org/content/early/2016/10/25/CIRCGENETICS.116.001515>

Data Supplement (unedited) at:

<http://circgenetics.ahajournals.org/content/suppl/2016/10/25/CIRCGENETICS.116.001515.DC1>

Permissions: Requests for permissions to reproduce figures, tables, or portions of articles originally published in *Circulation: Cardiovascular Genetics* can be obtained via RightsLink, a service of the Copyright Clearance Center, not the Editorial Office. Once the online version of the published article for which permission is being requested is located, click Request Permissions in the middle column of the Web page under Services. Further information about this process is available in the [Permissions and Rights Question and Answer](#) document.

Reprints: Information about reprints can be found online at:
<http://www.lww.com/reprints>

Subscriptions: Information about subscribing to *Circulation: Cardiovascular Genetics* is online at:
<http://circgenetics.ahajournals.org/subscriptions/>

SUPPLEMENTAL MATERIAL

Methods

Mouse Experiments. The mice were housed in the Medical College of Wisconsin Biological Resource Center, and all experiments were performed in accordance with an IACUC approved animal procedure protocol 1022. The *Snrk* cmcKO adult mice were generated from MYH6CRE positive *Snrk* LoxP/wild type (WT) males mated to *Snrk* LoxP/LoxP females. When possible age and litter matched male and female mice were used for each animal experiment. Mixed backcrossed animals were used for all of the mouse experiments. Primer information for mouse genotyping were provided previously¹.

Human Cardiomyocyte System. Directed differentiation of CMs from human embryonic stem cells (hESCs) is described in previous studies^{2,3}. Briefly, hESCs maintained on matrigel in mTeSR1 were dissociated into single cells using Accutase (Life Technologies) at 37°C for 5 min and then were seeded onto a matrigel-coated 12-well plate at 100,000-200,000 cell/cm² in mTeSR1 supplemented with 5 μ M Y-27632 (Tocris) for 24 h. After 24 h, fresh mTeSR1 medium was used every day to expand stem cells. When cells achieved a density of 500,000 cell/cm², cells were treated with 12 μ M CHIR99021 (Selleckchem) in RPMI/B27 without insulin for 24 h (day 0 to day 1). The medium was changed to RPMI/B27 without insulin on day 1, followed by 5 μ M IPW2 (Tocris) treatment on day 3. During the day 5 medium change IWP2 was removed. Cells were maintained in the RPMI/B27 starting from day 7, with the medium changed every 3 days.

Lentiviral Transduction of CMs and Drug Treatments. Day six CMs differentiated from hESCs were dissociated into single cells with Accutase at 37°C for 5-8 mins, and then were spun down into aliquots of 1.5×10^6 cells. Cells were re-suspended in 30 μ L concentrated lentivirus medium in the presence of 6 μ g/mL polybrene (Sigma), and then incubated at room temperature for 10 mins. At the end of

incubation, 2 mL of DMEM/10% FBS + 5 μ M Y-27632 (Tocris) was added and the suspension was transferred into 2 wells of a 12-well plate pre-coated with Matrigel, and incubated at 37°C, 5% CO₂ overnight. The medium was replaced with fresh DMEM/10% FBS on the second day of lentiviral infection, and afterwards cells were treated with water (control), and 5 μ M Y27632 for 9 days. Two days later, infected cells were selected and enriched for 3 days based on resistance to 1 μ g/mL puromycin (Sigma). 48 h before sample collection, cells were switched to RPMI containing B27 (no insulin) supplement. On day 15, the cells were rinsed with PBS and the proteins were collected for western blot analysis as previously described^{1,4,5}.

Echocardiography and Image Analysis. Transthoracic echocardiography was performed in anesthetized (2% isoflurane) six months old litter matched males. An investigator (L.M.H) who was blinded to the study groups performed the measurements and data analyses. A comprehensive 2D transthoracic echocardiogram with Doppler was performed on animals using Animals were studied with a commercially available echocardiographic system (Vivid 7, General Electric, Wauwatosa, WI), with an 11-MHz M12-L linear array transducer. A comprehensive 2D transthoracic echocardiogram with Doppler was performed from the cardiac short axis of the left ventricle at the papillary muscle level. Using the anatomical M-mode feature of the Vivid 7 echo, an M-mode display was generated from raw data 2D images of the short-axis of the left ventricle at the level of the papillary muscle with the line selected passing through the anterior and inferior segments. Ejection fraction % (EF) was measured using left ventricle end diastolic volume (LVEDV) and left ventricle end systolic volume (LVESV) using the formula $EF = \frac{LVEDV - LVESV}{LVEDV} \times 100$. Fractional shortening % (FS) was calculated with the formula: $left\ ventricle\ end\ diastolic\ dimension\ (LVEDD) - left\ ventricle\ end\ systolic\ dimension\ (LVESD) / LVEDD \times 100$. To assess diastolic function, pulse wave Doppler was used to assess transmitral inflow velocities in the apical 4-chamber view to obtain E velocities and isovolumic relaxation times (IVRT). Tissue Doppler was

used to assess tissue motion velocity from the mitral annulus to obtain e' velocities. E/e' is a calculated ratio. Pulse wave Dopplers was also used to sample velocities at the right ventricular outflow tract to assess for pulmonary acceleration time (PAT) and ejection time (ET). For two-dimensional strain analysis, the images were processed with EchoPac Q analysis software, (General Electric, Wauwatosa, WI). A cardiac cycle was defined from the peak of one R wave to the peak of the following R wave. Unless stated otherwise, for every measurement, three consecutive cardiac cycles were measured, and the average used for reporting. The method has been previously described⁶. Briefly, for radial and circumferential strain, the endocardial border was traced in an end-systolic frame in the short-axis view at the mid ventricle as identified by the prominent papillary muscles. The software automatically selected 6 equidistant tissue-tracking regions of interest in the myocardium. The outer border was adjusted to approximate the epicardial border. The computer then provided a profile of radial (myocardial deformation toward the center) and circumferential (myocardial deformation along the curvature) strain (%) with time.

Purification of SNRK. Cloned full length human SNRK sequence was transformed into BL21(DE3) competent cells (New England Biolabs). Bacterial cells were cultured overnight at 37°C in LB and induced with 1mM IPTG and incubated at 25°C for 6 h. The bacteria were then pelleted and the supernatant was removed. The pelleted bacteria were lysed using a bacterial lysis buffer containing 13 mL BPER (Pierce Technologies), 50 μ L DNase (2 U/ μ L), 41 μ L lysozyme (50 mg/mL) and 40 μ L 1M $MgCl_2$, protease inhibitor (Roche). The pellet was incubated with the lysis buffer at room temperature for 15 mins. One tablet of complete Mini EDTA-free protease inhibitor cocktail (Sigma) was add to the mixture and centrifuged at 7,600 x g for 15 mins. The supernatant was removed and dialyzed in a Slide-A-Lyzer with 10K molecular cutoff (ThermoFisher) overnight at room temperature in 1X binding buffer (57mM NaH_2PO_4 pH8.0, 300mM NaCl). The dialyzed supernatant was subjected to Nickel-NTA column

purification, and pure protein eluted in 10 mM, 25 mM and 250 mM Imidazole elution buffer. Samples of the fractions were resolved on a 10% Mini-PROTEAN TGX precast gel (BioRad), subjected to SDS-PAGE and subsequently stained with coomassie blue. Fractions eluted with 250 mM Imidazole were concentrated using Amicon Ultra 15 mL 50 MWL, kDa centrifugal filter units (EMD Millipore). Purified protein was subjected to Mass Spectrometry analysis for identity confirmation. SNRK kinase activity was confirmed using the ADP-Glo Kinase Assay (Promega). In short, purified SNRK protein was incubated with 10mM ATP, different amounts Histone H3 (0, 500ng, 1000ng, 2000ng, 4000ng) and kinase reaction buffer. ADP-Glo reagent was then added to stop the kinase reaction and deplete the unconsumed ATP. After 40 mins, the kinase detection reagent was added to convert the ADP to ATP for luciferase detection of the ATP. The luciferase was measured using a plate-reading luminometer (SpectraMaxGeminiEM, Molecular Devices) with SoftMax Pro software.

Identification of SNRK Candidate Substrates. All possible kinase substrates at each concentration of SNRK were evaluated by the Z-Factor rank within the array and were compared to the negative control assay. A protein was defined as being a candidate substrate for SNRK if it met the following conditions: 1) The Z-Factor, or signal-to-noise ratio, was greater than 0.35 on at least one assay, indicating a signal greater than 1.5-fold above the noise. 2) The Signal Used value was greater than 2,000 relative unites on at least one array probed with SNRK and was greater than 2-fold higher than the Signal Used value for the corresponding protein in the negative control assay. 3) The replicate spot coefficient of variation (CV) was less than 50% on the corresponding array. 4) The inter-assay CV was less than 50%.

Mass Spectral Analysis. Immunoprecipitated ROCK1 protein was incubated with or without 50 nM purified SNRK protein in the presence of 4 μ M ATP (Cell Biolabs) in kinase buffer [20 mM HEPES (pH 7.7), 20 mM MgCl₂, 2 mM DTT, 1X protease inhibitor (Roche) and 1X phosphatase inhibitor (Roche)]. The

samples were allowed to incubate for 15 mins at 30°C. After incubation the samples were washed 2-3 times with kinase buffer and re-suspended in Lamelli sample buffer. The samples were resolved using gel electrophoresis and then subjected to in-gel tryptic digestion followed by Mass Spectral analysis.

Mass spectral analysis was performed on an LTQ-Orbitrap Velos mass spectrometer (Thermo Scientific, Waltham, MA, USA) coupled with a nanoAQUITY ultraperformance liquid chromatographer (UPLC) (Waters Corp.) interfaced with a nanoelectrospray ion source. Peptide separation was carried out on a capillary column built in-house with 5µm C18 nanoparticles to 10 cm long column with 75 µm inner diameter tubing. The fused silica capillaries (Polymicro Technologies, Phoenix, AZ, USA) for the columns were pulled by a micropipette puller P-2000 (Sutter Instrument Company, CA, USA) and packed with C18 resin using a bomb-loader. The solvents A and B used for chromatographic separation of peptides were 2% acetonitrile in 0.1% formic acid and 98% acetonitrile in 0.1% formic acid, respectively. The peptides injected onto the microcapillary column were resolved at the rate of 200 nl/min, using the following gradient conditions: 0 to 10 min, 2 to 20% B; 120 min, 40% B; 135 min, 60% B; 150 min, 70% B; 158 min, 98%B, which was held for 4 min and then switched to 98% A and held for another 18 min. The ions eluted from the column were electrosprayed at a voltage of 1.70 kV. The ion transfer temperature was kept at 250°C. No auxiliary or sheath gas was used.

Survey full-scan mass spectrometry (MS) spectra (m/z , 300 to 2,000) were recorded in the Orbitrap analyzer at a resolution of 30,000 followed by tandem mass spectrometry (MS/MS) of the 10 most intense peptide ions in the linear ion trap analyzer. Neutral loss-triggered multistage activation for simultaneous fragmentation of neutral loss product and precursor was enabled at m/z of -98, -49 and -32.6 relative to the precursor ion, corresponding to a neutral loss of phosphate moiety from +1, +2, and +3 charged ions. The chromatographic and mass spectral functions were controlled using the Xcalibur data system (ThermoFinnigan, Palo Alto, CA, USA). Peptides were identified using the Mascot search

algorithm for human protein database at a global false-discovery rate of 5%. The resulting files were evaluated using Visualize tool⁷.

Tissue Sectioning, Staining and Image Analysis. Adult mouse hearts were fixed in 4% paraformaldehyde/PBS for 1 to 2 days at 4°C. After fixation tissues were washed extensively in PBS and embedded in paraffin or sucrose/OCT as previously described¹. Seven micron thick sections were stained with Gomori's Trichrome staining and Hematoxylin counter staining. The microscopic images of the entire tissue section were scanned at 40x magnification using the Nanozoomer 2.0-HT (Hamamatsu, Japan) digital slide scanning system (Children's Research Institute's Imaging Core). The amount of fibrosis was quantified using software assisted, unbiased microimage quantification method. The scanned images were imported into Visiopharm software (Denmark) and using the imager module, three 20x ROI images were extracted from left, center and right regions of the heart. Collagen positive regions (navy blue stains) were identified by thresholding the specific image channel filter and the rest of the tissue (muscle - stained red and nucleus - stained deep blue) classified as tissue region with total tissue region defined as sum of muscle, nuclear and collagen region without any interstitial space. All original images were processed with this preset thresholds and linear Bayesian classification to generate a processed image. Total collagen positive area per ROI was measured in microns and represented as a percentage of the total tissue area.

References

1. Cossette SM, Gastonguay AJ, Bao X, Lerch-Gaggl A, Zhong L, Harmann LM, et al. Sucrose non-fermenting related kinase enzyme is essential for cardiac metabolism. *Biol Open*. 2014;BIO20149811.

2. Lian X, Hsiao C, Wilson G, Zhu K, Hazeltine LB, Azarin SM, et al. Robust cardiomyocyte differentiation from human pluripotent stem cells via temporal modulation of canonical wnt signaling. *Proc Nat Acad Sci U S A*. 2012;109:E1848-1857.
3. Lian X, Zhang J, Azarin SM, Zhu K, Hazeltine LB, Bao X, et al. Directed cardiomyocyte differentiation from human pluripotent stem cells by modulating wnt/beta-catenin signaling under fully defined conditions. *Nat Protoc*. 2013;8:162-175.
4. Bao X, Lian X, Dunn KK, Shi M, Han T, Qian T, et al. Chemically-defined albumin-free differentiation of human pluripotent stem cells to endothelial progenitor cells. *Stem Cell Res*. 2015;15:122-129.
5. Lian X, Bao X, Zilberter M, Westman M, Fisahn A, Hsiao C, et al. Chemically defined, albumin-free human cardiomyocyte generation. *Nat Methods*. 2015;12:595-596.
6. Migrino RQ, Zhu X, Pajewski N, Brahmabhatt T, Hoffmann R, Zhao M. Assessment of segmental myocardial viability using regional 2-dimensional strain echocardiography. *J Am Soc Echocardiogr*. 2007;20:342-351.
7. Halligan BD, Greene AS. Visualize: A free and open source multifunction tool for proteomics data analysis. *Proteomics*. 2011;11:1058-1063.

Supplemental Figures and Tables

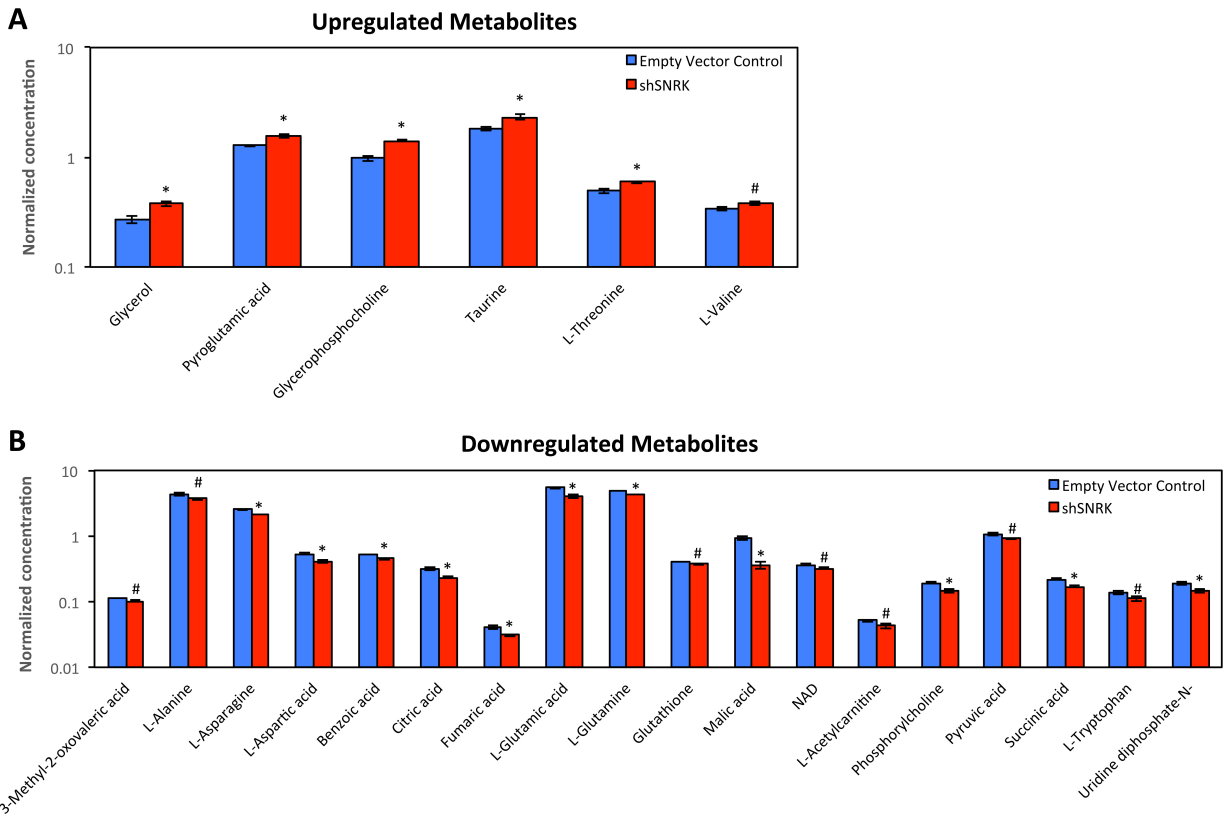


Figure S1. Loss of SNRK in cardiomyocytes results in altered metabolic profiles. Panel A shows the upregulated metabolites and B shows the downregulated metabolites. * $p < 0.05$, # $p < 0.1$.

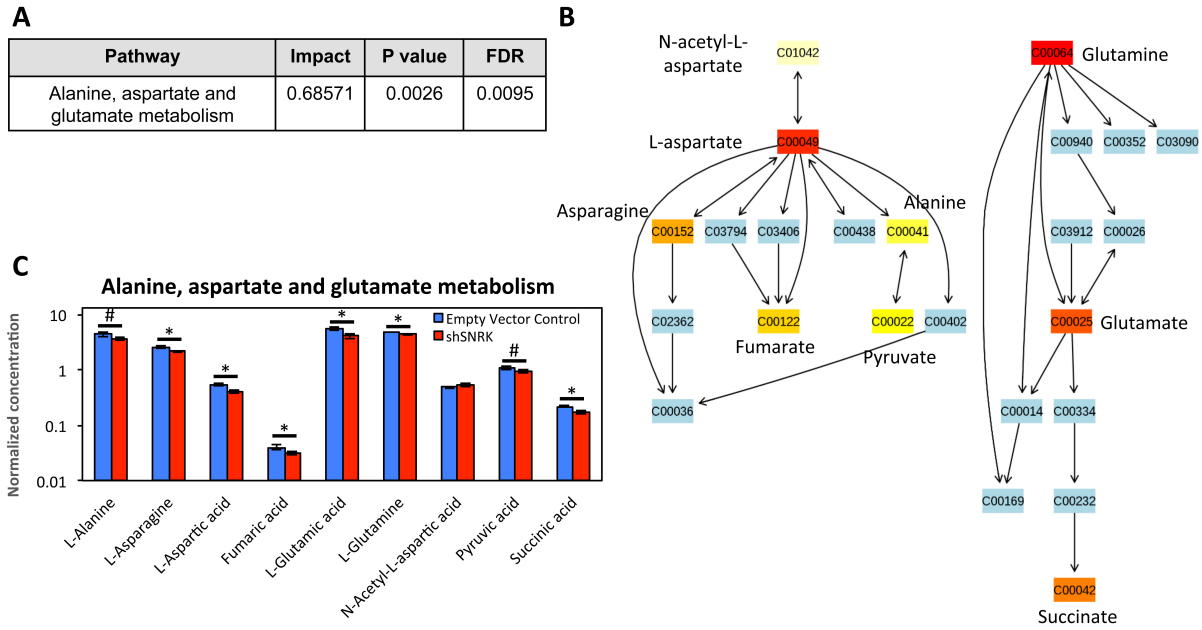


Figure S2. Loss of SNRK in cardiomyocytes results in altered alanine, aspartate, and glutamate metabolism. Panel A is the Pathway topology analysis impact score, p value and FDR. Panel B is the pathway view showing the corresponding Alanine, aspartate and glutamate metabolic pathways. The matched metabolites are highlighted according to their *P* values. Panel C is the normalized concentration from the individual metabolites. **p*<0.05, # *p*<0.1.

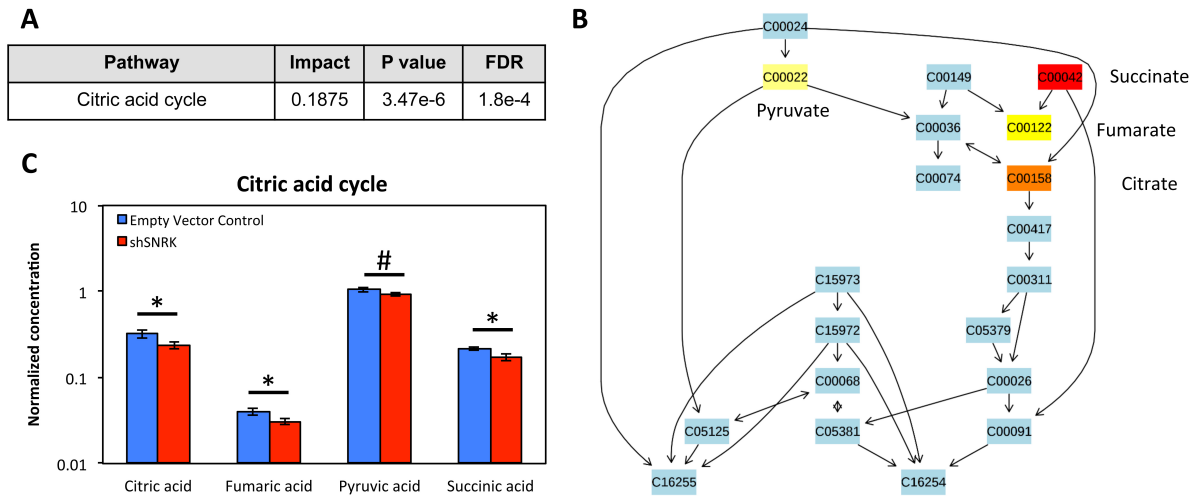


Figure S3. Loss of SNRK in cardiomyocytes results in altered Citric acid cycle metabolites. Panel A is the Pathway topology analysis impact score, p value and FDR. Panel B is the pathway view showing the altered metabolites in the citric acid cycle. The matched metabolites are highlighted according to their *P* values. Panel C is the normalized concentration from the individual metabolites. **p*<0.05, # *p*<0.1.

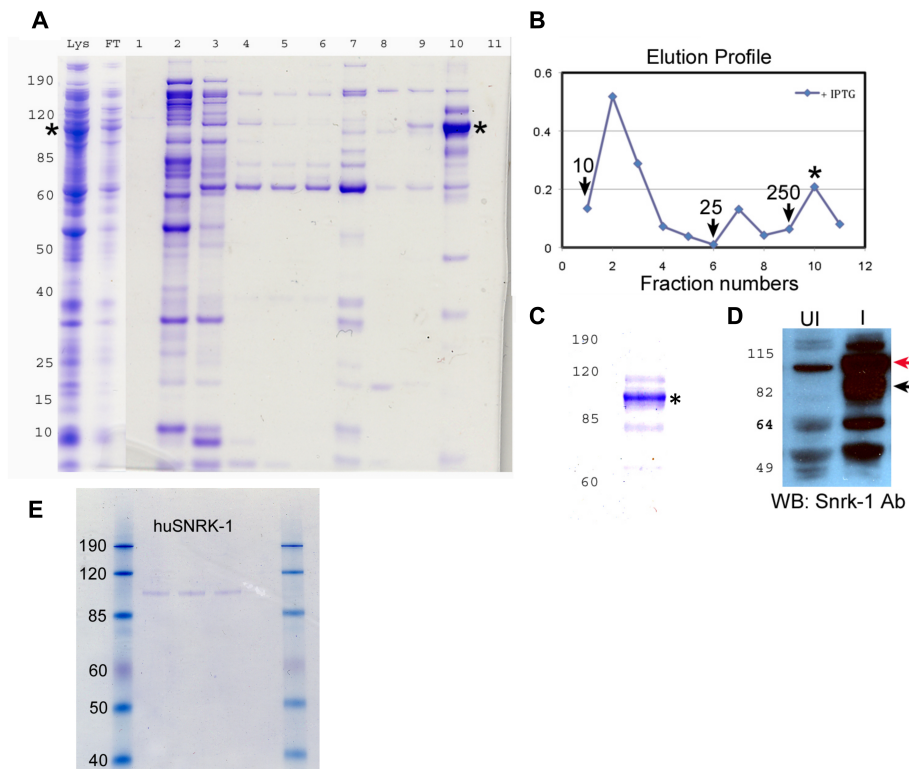


Figure S4. Human histidine tagged SNRK protein generation and purification. Panel A indicates a SDS-PAGE gel resolving the different fractions. Lys: lysate, FT: flow through. Numbers indicate the fraction number post 10 mM (1-5), 25 mM (6-8) and 250 mM (9-11) imidazole elution. The numbers on top of each lane corresponds to fraction elution profile in panel B. Panel B indicates elution profile and arrows indicate imidazole elution points with each number corresponding to concentration of imidazole. Only IPTG induced bacterial profile is shown. Panel C shows fraction #10 (black asterisks), re-purified a second round on Nickel NTA column and eluted with 250 mM imidazole. Panel D shows a western blot with SNRK antibody in uninduced (UI) and induced (I) lysate. Red arrow indicates the full-length protein and black arrow indicates degraded products. Numbers on left of each gel indicate protein size markers in kDa. Panel E indicates the three fractions from 250 mM imidazole purification that were subsequently concentrated and run on Coomassie-stained SDS-PAGE gel before the final product was sent for array experiment.

1	M ST GDSFETR	FEKMDNLLRD	PKSEVI S ICL	LDGLDALVYD	LDFPALRKNK
51	NIDN FLSRYK	DTINKIRDLR	MKAEDY EVVK	VIGR GAFGEV	QLVR HKSTRK
101	VYAMKLLSK F	EMIKR SDSA F	FWEER DIMAF	ANSP WV Q LF	YAFQ DDRYLY
151	MVMEYMPGGD	LVNLM S NYDA	PEKWARFYTA	EVVLALDAIH	SMGFIHG DV K
201	PDNML LDK S G	HLKL ADFGTR	MKM NKEGMVR	CDTAV (T)DY	ISPE VLKSQ G
251	GDGY Y GRECD	WWSVG V FLYE	MLVGDTPFYA	D S LVGTYSKI	MNHK N SLTF P
301	DDND ISKEAK	NLIC AF L TD R	EVRL GRNGVE	EIKR H L FFKN	DQWA WETLRD
351	TVAP VVPDLS	SDID TSNFDD	LEED KGEEET	FPI PKAFVGN	QLP FVGFT Y Y
401	SNRR YLS S AN	PNDN RTSSNA	DKSL QES L OK	TIYK LEE Q LH	NEM QLKDEME
451	QKCR TSNIKL	DKIM KELDEE	GNQR N L (S) T	VSQI EKEKML	LQHR INEYOR
501	KAEQENEKRR	NVNE VSTLK	NQLE DLKKVS	QN S OLANEKL	SQLOKQLEEA
551	NDLLR T ESDT	AVRLR K S H TE	MSKS I S QLES	LNRELQERNR	ILENSKSQTD
601	KD Y Y Q LQAIL	EAERRDRGHD	SEMIGDLQAR	ITSLQEEVKH	LKH N LEKVEG
651	ERKE AQ DMLN	HSEK EKNLE	IDLNYKL S L	QORLEQEVNE	HKVTKARLTD
701	KHQSIEEAK S	VAMCEMEK K L	KEEREAREKA	ENRVVQIE Q	C S M LDV D LKQ
751	SQOKLEHLTG	NKERMEDEVK	NLTLQLEQES	NKRLLLQNEL	KTQAF E ADNL
801	KGLEKQMKQE	INTLLEAKRL	LEFELAQLTK	QYRGNEGQMR	ELQDQLEAEQ
851	YFSTLYKTQV	KELKEEIEEK	NREN L KKI Q E	LQNEKET L AT	QLDLA E TKAE
901	SEQLARGLLE	EQ Y FEL T QES	KKAASRN Q E	ITDKDHTVSR	LEEANSMLTK
951	DIEILRRENE	ELTERM K KAE	EEYKLEKEE E	ISNLKAAFEK	NINTERTLKT
1001	QAVNKLA E IM	NRKDFKIDRK	KAN T QDLR K K	EKENRKLQLE	LNQEREKFNQ
1051	MVVKHQKELN	DMQAQLVEEC	AHR N EL Q M L	ASKE SDIEQL	RAKLLD L SD S
1101	TSV AS F PSAD	ETD GNLPESR	IEG W LSVPNR	GNIKRYGWKK	QYVVVSSK K I
1151	LF Y NDEQDKE	QSNPSMVLDI	DKLFHVR P T	QGDVYRA E TE	EIPKIFQILY
1201	ANE G E C RKDV	EMEPVQQA E K	TNFQNHKGHE	FIPTLYHFPA	NCDACAKPLW
1251	HVFKPPP A LE	CRRCHVK C HR	DHLDKKEDLI	CPCKV S Y D VT	SARD M L L L L A C
1301	SQDE QKKWVT	HLVKK I PK N P	P S G FVRASPR	T I S T S TANQ	SFRKVVKNTS
1351	G K (S)				

Match to ROCK1_HUMAN (Q13464 UniProtKB) Score: 1535

Sequence Coverage: 29%

-  PhosphoID in current study
-  Phosphorylation confirmed by Site Directed Mutagenesis
-  Reported in literature to induce enzymatic activity in rat and mouse (S1333)
-  Previously identified by Proteomics

Matched peptides shown in Bold Red

Figure S5. Mass spectral (MS) analysis of the SNRK mediated phosphorylation sites on ROCK1. MS

analysis was used to identify the residues on ROCK which are phosphorylated by SNRK in vitro. Full length ROCK was incubated with or without SNRK. The SNRK dependent phosphorylated residues are depicted with a blue circle and the previously published phosphorylated residues are depicted with a magenta circle. MS identified amino acids are shown in bold red (current study), and the yellow highlighted residues were previously identified but not yet confirmed by proteomic analysis on PhosphoSitePlus.

Trichome Staining

Genotype	Average % Collagen
CRE Negative 1	6.60
CRE Negative 2	7.24
CRE Negative 3	12.25
CRE Negative 4	15.45
Average	10.38
SEM	2.07
MYH6CRE SNRK L/L 1	17.62
MYH6CRE SNRK L/L 2	21.70
MYH6CRE SNRK L/L 3	18.63
Average	19.32
SEM	1.23

Adult Heart Lysate Western Blot Quantification

% Relative Intensity	Ratio					
	ROCK1/Tubulin	ROCK2/Tubulin	pMBS/MBS	pERK/ERK	pAKT/AKT	pIKK/IKK
Genotype						
CRE Negative 1	100.00	100.00	100.00	100.00	100.00	100.00
CRE Negative 2	105.91	129.55	105.39	118.63	100.26	101.15
CRE Negative 3	94.09	70.45	94.61	81.37	99.74	98.85
Average	100.00	100.00	100.00	100.00	100.00	100.00
SEM	3.41	17.06	3.11	10.75	0.15	0.66
MYH6CRE SNRK L/L 1	68.89	96.79	121.84	168.36	41.77	23.39
MYH6CRE SNRK L/L 2	123.78	107.34	112.14	105.87	67.13	51.21
MYH6CRE SNRK L/L 3	76.34	55.27	134.66	276.17	29.53	59.24
Average	89.67	86.47	122.88	183.47	46.15	44.62
SEM	17.19	15.89	6.52	49.74	11.07	10.86

Cardiomyocyte Lysate Western Blot Quantification

% Relative Intensity	Ratio			
Genotype	pMBS/MBS	pAKT/AKT	pIKK/IKK	pERK/ERK
Non-Sliencing-Control 1	100.00	100.00	100.00	100.00
Non-Sliencing-Control 2	100.00	100.00	100.00	100.00
Non-Sliencing-Control 3	100.00	100.00	100.00	100.00
Non-Sliencing-Control 4	No Sample	100.00	No Sample	100.00
Average	100.00	100.00	100.00	100.00
SEM	0.00	0.00	0.00	0.00
Non-Sliencing-Rock Inh 1	35.48	744.30	78.44	88.78
Non-Sliencing-Rock Inh 2	99.99	337.96	268.41	193.19
Non-Sliencing-Rock Inh 3	64.57	16.79	244.95	61.88
Non-Sliencing-Rock Inh 4	No Sample	No Sample	No Sample	27.17
Average	66.68	366.35	197.27	92.75
SEM	18.65	210.49	59.80	35.78
shSNRK-Control 1	83.02	168.95	249.50	545.89
shSNRK-Control 2	161.12	280.99	318.23	335.43
shSNRK-Control 3	125.92	81.92	195.43	70.86
shSNRK-Control 4	No Sample	161.20	No Sample	46.28
Average	123.35	173.26	254.39	249.62
SEM	22.58	40.94	35.54	118.48
shSNRK-Rock Inh 1	8.24	301.99	344.53	19.71
shSNRK-Rock Inh 2	56.12	118.15	653.82	80.37
shSNRK-Rock Inh 3	57.90	9.26	176.38	32.75
shSNRK-Rock Inh 4	No Sample	No Sample	No Sample	8.58
Average	40.75	143.13	391.58	35.36
SEM	16.26	85.42	139.82	15.80

Table S1. Individual data values for the Trichome staining and Western blot analysis.

Sample ID	3-Methyl-2-oxovaleric acid	Acetic acid	L-Alanine	L-Arginine	L-Asparagine	L-Aspartic acid	Benzoic acid	Choline	Citric acid	Creatine
CNT-1	0.11	4.66	4.48	1.83	2.62	0.52	0.54	0.13	0.36	0.08
CNT-2	0.12	4.39	3.90	2.01	2.41	0.52	0.51	0.12	0.29	0.11
CNT-3	0.11	4.50	4.75	1.88	2.70	0.56	0.54	0.14	0.32	0.12
Average	0.11	4.52	4.38	1.91	2.58	0.54	0.53	0.13	0.32	0.10
SEM	0.00	0.08	0.25	0.05	0.09	0.01	0.01	0.01	0.02	0.01
shSNRK-1	0.11	4.64	3.87	1.93	2.23	0.44	0.48	0.15	0.24	0.17
shSNRK-2	0.10	3.90	3.80	1.84	2.16	0.40	0.47	0.14	0.21	0.16
shSNRK-3	0.10	4.48	3.37	1.65	2.06	0.38	0.42	0.14	0.25	0.08
Average	0.10	4.34	3.68	1.80	2.15	0.41	0.46	0.14	0.23	0.14
SEM	0.00	0.22	0.16	0.08	0.05	0.02	0.02	0.00	0.01	0.03
Sample ID	Phosphocreatine	Formic acid	Fumaric acid	D-Glucose	L-Glutamic acid	L-Glutamine	Glutathione	Glycerol	Glycine	Isobutyric acid
CNT-1	0.12	2.78	0.04	1.28	5.88	4.74	0.41	0.31	3.26	0.03
CNT-2	0.13	2.48	0.04	0.73	5.15	4.87	0.42	0.27	3.14	0.03
CNT-3	0.19	2.53	0.04	0.65	5.48	4.88	0.41	0.24	3.39	0.04
Average	0.15	2.60	0.04	0.89	5.50	4.83	0.41	0.27	3.26	0.03
SEM	0.02	0.09	0.00	0.20	0.21	0.04	0.00	0.02	0.07	0.00
shSNRK-1	0.17	2.95	0.03	0.64	4.37	4.34	0.40	0.35	3.56	0.06
shSNRK-2	0.19	2.57	0.03	0.48	4.04	4.42	0.36	0.41	3.32	0.04
shSNRK-3	0.11	2.75	0.03	0.75	3.62	4.22	0.38	0.37	3.16	0.04
Average	0.16	2.76	0.03	0.62	4.01	4.33	0.38	0.38	3.35	0.05
SEM	0.02	0.11	0.00	0.08	0.22	0.06	0.01	0.02	0.11	0.01

Sample ID	L-Isoleucine	L-Lactic acid	L-Leucine	L-Lysine	Malic acid	L-Methionine	Myoinositol	N-Acetyl-L-aspartic acid	NAD	L-Acetylcarnitine
CNT-1	0.81	42.69	0.56	0.38	0.92	0.26	3.76	0.51	0.35	0.05
CNT-2	0.85	46.56	0.63	0.46	0.83	0.25	2.97	0.46	0.38	0.05
CNT-3	0.84	42.72	0.62	0.40	1.07	0.28	3.75	0.48	0.36	0.05
Average	0.83	43.99	0.60	0.41	0.94	0.26	3.49	0.48	0.36	0.05
SEM	0.01	1.29	0.02	0.02	0.07	0.01	0.26	0.01	0.01	0.00
shSNRK-1	0.79	44.02	0.61	0.42	0.30	0.26	4.29	0.55	0.34	0.05
shSNRK-2	0.84	47.45	0.67	0.40	0.43	0.29	3.80	0.48	0.30	0.04
shSNRK-3	0.92	47.92	0.72	0.44	0.33	0.27	4.05	0.57	0.33	0.04
Average	0.85	46.47	0.67	0.42	0.36	0.27	4.05	0.53	0.32	0.04
SEM	0.04	1.23	0.03	0.01	0.04	0.01	0.14	0.03	0.01	0.00
Sample ID	Phosphorylcholine	O-Phosphoethanolamine	Pantothenic acid	L-Phenylalanine	L-Proline	Pyroglutamic acid	Pyruvic acid	L-Serine	Glycero-phosphocholine	Succinic acid
CNT-1	0.20	4.11	0.09	0.25	1.66	1.25	1.07	1.13	0.88	0.21
CNT-2	0.19	3.92	0.10	0.29	1.61	1.30	1.13	1.00	1.01	0.23
CNT-3	0.18	4.28	0.08	0.29	1.73	1.27	0.99	1.08	1.03	0.22
Average	0.19	4.10	0.09	0.27	1.67	1.27	1.06	1.07	0.97	0.22
SEM	0.01	0.11	0.00	0.01	0.04	0.02	0.04	0.04	0.05	0.01
shSNRK-1	0.16	4.53	0.08	0.24	1.85	1.56	0.99	1.01	1.45	0.17
shSNRK-2	0.15	4.34	0.09	0.27	1.77	1.44	0.90	0.94	1.41	0.19
shSNRK-3	0.12	4.18	0.08	0.26	1.63	1.67	0.89	1.06	1.37	0.16
Average	0.14	4.35	0.08	0.26	1.75	1.56	0.93	1.01	1.41	0.17
SEM	0.01	0.10	0.00	0.01	0.06	0.07	0.03	0.03	0.02	0.01

Sample ID	Taurine	L-Threonine	Trans-4-Hydroxy-L-proline	L-Tryptophan	L-Tyrosine	Uridine diphosphate-N-acetylglucosamine	L-Valine
CNT-1	1.86	0.55	1.27	0.13	0.25	0.19	0.31
CNT-2	1.64	0.47	0.95	0.15	0.25	0.17	0.35
CNT-3	1.98	0.48	1.20	0.13	0.24	0.21	0.36
Average	1.83	0.50	1.14	0.14	0.25	0.19	0.34
SEM	0.10	0.03	0.10	0.01	0.00	0.01	0.01
shSNRK-1	2.55	0.55	1.09	0.12	0.26	0.16	0.36
shSNRK-2	2.32	0.61	0.85	0.10	0.28	0.13	0.37
shSNRK-3	2.11	0.61	0.87	0.11	0.23	0.15	0.40
Average	2.33	0.59	0.94	0.11	0.26	0.14	0.38
SEM	0.13	0.02	0.08	0.01	0.01	0.01	0.01

Table S2. Individual data values for the Metabolomics data analysis.

Compound Name	HMDB	Fold change	pvalue	Compound Name	HMDB	Fold change	pvalue
3-Methyl-2-oxovaleric acid	HMDB00491	-1.1045	0.0579	L-Leucine	HMDB00687	1.1034	0.1765
4-Hydroxyproline	HMDB00725	-1.2171	0.1779	L-Lysine	HMDB00182	1.0209	0.7521
Acetic acid	HMDB00042	-1.0403	0.5029	L-Methionine	HMDB00696	1.0318	0.5483
Benzoic acid	HMDB01870	-1.1618	0.0293	L-Phenylalanine	HMDB00159	-1.0657	0.3195
Choline	HMDB00097	1.0970	0.1850	L-Proline	HMDB00162	1.0506	0.3155
Citric acid	HMDB00094	-1.3709	0.0187	L-Serine	HMDB00187	-1.0653	0.2615
Creatine	HMDB00064	1.3478	0.2904	L-Threonine	HMDB00167	1.1904	0.0452
D-Glucose	HMDB00122	-1.4290	0.2758	L-Tryptophan	HMDB00929	-1.2443	0.0691
Formic acid	HMDB00142	1.0608	0.3383	L-Tyrosine	HMDB00158	1.0252	0.6969
Fumaric acid	HMDB00134	-1.2891	0.0320	L-Valine	HMDB00883	1.1174	0.1000
Glutathione	HMDB00125	-1.0884	0.0604	Malic acid	HMDB00744	-2.6446	0.0018
Glycerol	HMDB00131	1.3832	0.0170	Myoinositol	HMDB00211	1.1585	0.1364
Glycerophosphocholine	HMDB00086	1.4451	0.0012	N-Acetyl-L-aspartic acid	HMDB00812	1.1035	0.1920
Glycine	HMDB00123	1.0256	0.5675	NAD	HMDB00902	-1.1205	0.0677
Isobutyric acid	HMDB01873	1.3424	0.1492	O-Phosphoethanolamine	HMDB00224	1.0601	0.1671
L-Acetylcarnitine	HMDB00201	-1.2026	0.0890	Pantothenic acid	HMDB00210	-1.0767	0.3511
L-Alanine	HMDB00161	-1.1898	0.0777	Phosphocreatine	HMDB01511	1.0772	0.7406
L-Arginine	HMDB00517	-1.0563	0.3586	Phosphorylcholine	HMDB01565	-1.3449	0.0126
L-Asparagine	HMDB00168	-1.1999	0.0135	Pyroglutamic acid	HMDB00267	1.2219	0.0139
L-Aspartic acid	HMDB00191	-1.3150	0.0044	Pyruvic acid	HMDB00243	-1.1466	0.0589
L-Glutamic acid	HMDB00148	-1.3717	0.0079	Succinic acid	HMDB00254	-1.2730	0.0104
L-Glutamine	HMDB00641	-1.1167	0.0024	Taurine	HMDB00251	1.2745	0.0350
L-Isoleucine	HMDB00172	1.0221	0.6772	Uridine diphosphate-N-acetylglucosamine	HMDB00290	-1.3140	0.0225
L-Lactic acid	HMDB00190	1.0563	0.2365				

Table S3. Full metabolomic data set. HMDB: human metabolic database ID number.

Database ID	Ultimate ORF ID	Signal Used	Z-Factor	Z-Score	CI P-Value	Replicate Spot CV	Interassay CV	Assay	Signal Used Neg	Ratio to Neg	Description
IC036089.1	IOH27267	2714	0.71	0.92	5.27E-02	5%	33%	50 nM	31	87.7	MLLT3
IC000250.1	IOH4515	4650	0.79	1.76	1.75E-02	5%	3%	50 nM	1423	3.3	NME3
IC000633.1		37106	0.54	12.01	7.75E-04	11%	0%	5 nM	6431	5.8	TTK
IC000633.1		10465	0.84	4.31	2.98E-03	4%	2%	50 nM	4132	2.5	TTK
IC005403.1	IOH61712	2200	0.65	0.70	7.47E-02	6%	10%	50 nM	887	2.5	C11orf57
IC008668.1	IOH9808	15077	0.86	4.71	4.25E-03	3%	9%	5 nM	4132	3.6	GAK
IC008668.1	IOH9808	2758	0.78	0.94	4.37E-02	2%	4%	50 nM	1181	2.3	GAK
IC010357.1	IOH14260	3147	0.58	1.11	3.72E-02	9%	5%	50 nM	842	3.7	RSRC1
IC012576.1	IOH12217	3144	0.62	1.11	4.10E-02	8%	26%	50 nM	1134	2.8	BAZ2B
IC014298.1	IOH13449	2232	0.70	0.71	8.14E-02	7%	0%	50 nM	620	3.6	PRKRIP1
IC016330.1	IOH14709	3175	0.82	1.12	3.60E-02	1%	37%	50 nM	606	5.2	RAD51AP1
IC017070.1	IOH11214	2106	0.85	0.66	7.54E-02	1%	14%	50 nM	521	4.0	CLUAP1
IC020726.1	IOH12969	2249	0.60	0.45	2.13E-01	2%	3%	5 nM	753	3.0	SCEL
IC020810.1	IOH27927	17729	0.97	7.46	1.09E-03	1%	3%	50 nM	8713	2.0	CHD2
IC024208.1	IOH12635	3825	0.85	1.41	2.24E-02	2%	5%	50 nM	1788	2.1	RBM23
IC036434.1	IOH62212	4915	0.88	1.34	4.02E-02	0%	4%	5 nM	1446	3.4	VRK2
IC053878.1	IOH28978	19734	0.60	6.25	2.69E-03	9%	7%	5 nM	3803	5.2	ZAP70
IC057783.1	IOH29271	6275	0.77	2.48	8.68E-03	6%	6%	50 nM	2768	2.3	SFRS2B
JM_001005158.1	IOH57124	16956	0.96	7.14	1.07E-03	1%	2%	50 nM	8020	2.1	SFMBT1
JM_001204.3		3430	0.42	0.81	4.17E-02	1%	12%	5 nM	841	4.1	BMPR2
JM_001396.2		7538	0.93	2.21	1.68E-02	1%	6%	5 nM	3478	2.2	DYRK1A
JM_002005.2	IOH21035	5454	0.48	1.52	4.08E-02	15%	9%	5 nM	1402	3.9	FES
JM_002031.2	IOH56137	9494	0.70	2.85	1.18E-02	9%	0%	5 nM	2768	3.4	FRK
JM_002031.2	IOH56137	3096	0.68	1.09	3.69E-02	6%	2%	50 nM	1315	2.4	FRK
JM_002904.4	IOH14621	2048	0.46	0.39	2.93E-01	9%	17%	5 nM	1003	2.0	RDBP
JM_003609.2	IOH4232	3524	0.47	1.27	3.02E-02	4%	2%	50 nM	984	3.6	HIRIP3
JM_004103.2		3888	0.81	1.00	6.82E-02	3%	11%	5 nM	664	5.9	PTK2B
JM_005197.2	IOH56874	7269	0.77	2.91	6.37E-03	6%	8%	50 nM	3354	2.2	FOXN3
JM_005902.1	IOH27044	5846	0.58	2.28	1.05E-02	2%	9%	50 nM	1420	4.1	SMAD3
JM_005902.1	IOH27044	4092	0.58	1.06	6.83E-02	10%	1%	5 nM	1181	3.5	SMAD3
JM_006399.2	IOH21626	6765	0.49	2.69	9.05E-03	12%	4%	50 nM	2400	2.8	BATF
JM_007026.1	IOH21130	5090	0.65	1.40	4.22E-02	8%	1%	5 nM	842	6.0	DUSP14
JM_007026.1	IOH21130	2328	0.39	0.75	7.20E-02	4%	1%	50 nM	673	3.5	DUSP14
JM_007067.3	IOH21942	7049	0.86	2.82	6.54E-03	3%	1%	50 nM	3298	2.1	MYST2
JM_014840.2	IOH36839	17020	0.68	5.35	3.45E-03	6%	10%	5 nM	4972	3.4	NUAK1
JM_015191.1	IOH45349	20216	0.83	6.09	1.17E-03	3%	2%	5 nM	3835	5.3	SNF1LK2
JM_015191.1	IOH45349	14831	0.84	6.21	1.49E-03	5%	4%	50 nM	3204	4.6	SNF1LK2
JM_015640.1	IOH22934	3931	0.74	0.96	3.38E-02	5%	16%	5 nM	1792	2.2	SERP1 transcript variant 4
JM_015978.1		3943	0.53	1.46	2.19E-02	5%	11%	50 nM	1180	3.3	TNNI3K
JM_015978.1		4746	0.58	1.22	2.52E-02	11%	19%	5 nM	1788	2.7	TNNI3K

JM_016072.2	IOH10546	2213	0.40	0.70	7.53E-02	0%	2%	50 nM	986	2.2	GOLT1B
JM_016440.1		2296	0.51	0.47	2.14E-01	5%	4%	5 nM	1117	2.1	VRK3
JM_016542.2	IOH39650	13193	0.46	4.08	6.85E-03	17%	10%	5 nM	5936	2.2	MST4 transcript variant 1
JM_017588.1	IOH4895	2681	0.64	0.60	1.54E-01	5%	2%	5 nM	933	2.9	WDR5 transcript variant 1
JM_018328.1	IOH12893	2155	0.66	0.42	2.49E-01	5%	6%	5 nM	289	7.4	MBD5
JM_022073.1	IOH13327	6798	0.67	1.86	1.17E-02	9%	0%	5 nM	1423	4.8	EGLN3
JM_022073.1	IOH13327	23848	0.78	10.15	5.61E-04	3%	23%	50 nM	6431	3.7	EGLN3
JM_024039.1	IOH4379	3950	0.64	1.46	2.21E-02	6%	3%	50 nM	1310	3.0	MIS12
JM_078630.1	IOH37755	2307	0.49	0.74	7.78E-02	8%	11%	50 nM	930	2.5	MSL3L1 transcript variant 2
JM_152789.1	IOH21683	11585	0.80	4.80	2.47E-03	5%	3%	50 nM	940	12.3	FAM133B transcript variant 1
'3049		37904	0.81	12.27	6.91E-04	6%	6%	5 nM	17278	2.2	ABL1 transcript variant a
'V3500		14551	0.89	4.53	4.54E-03	3%	14%	5 nM	5279	2.8	CSNK1E transcript variant 2
'V3504		25678	0.71	8.22	1.59E-03	9%	0%	5 nM	8713	2.9	TBK1
'V3504		3472	0.84	1.25	3.08E-02	3%	45%	50 nM	1626	2.1	TBK1
'V3691		20367	0.69	6.13	1.22E-03	6%	21%	5 nM	940	21.7	ROCK1
'V3691		3144	0.88	1.11	3.27E-02	0%	1%	50 nM	1120	2.8	ROCK1
'V3810		9817	0.72	2.96	9.80E-03	1%	27%	5 nM	3634	2.7	MINK1 transcript variant 4
'V3824		4272	0.63	1.07	3.00E-02	9%	14%	5 nM	1922	2.2	GRK5
'V3836		15152	0.68	4.73	4.65E-03	10%	11%	5 nM	3204	4.7	IKBKB
'V3836		2695	0.89	0.91	4.53E-02	1%	15%	5 nM	990	2.7	IKBKB
'V3864		17281	0.91	5.16	1.60E-03	2%	9%	50 nM	8020	2.2	ABL1 transcript variant a; mutant E255K
'V3864		7745	0.65	3.12	5.81E-03	8%	8%	50 nM	3755	2.1	ABL1 transcript variant a
'V3869		4017	0.79	1.04	6.30E-02	2%	5%	5 nM	1654	2.4	KIT transcript

											variant 1; mutant T670I
V4211		9708	0.47	2.93	1.13E-02	9%	5%	5 nM	2400	4.0	MAP4K2
V4211		2293	0.78	0.74	6.62E-02	4%	23%	50 nM	647	3.5	MAP4K2
V4792		26922	0.84	8.20	6.80E-04	5%	17%	5 nM	8002	3.4	SNF1LK2
V4877		6157	0.71	1.75	2.83E-02	8%	20%	5 nM	1608	3.8	ACVR1
V4883		2994	0.61	0.67	6.19E-02	8%	10%	5 nM	1079	2.8	ACVRL1
M_378350.2	IOH43457	4789	0.85	1.30	4.34E-02	2%	46%	5 nM	2344	2.0	LOC400027

Table S4. Putative SNRK targets identified in the human ProtoArray microarray.

		IVSd/ BW cm/g	LVIDd/B W cm/g	LVPWd/ BW cm/g	LVIDs/ BW cm/g	EDV/ BW ml/g	EDV/ BW ml/g	EF %	% FS	SVI ml/g
Baseline	WT-Fasudil SEM	0.0038 0.0001	0.0162 0.0008	0.0035 0.0004	0.0113 0.0008	0.0061 0.0004	0.0028 0.0004	65.1820 2.5973	30.8120 1.7259	0.0038 0.0003
	WT-Saline SEM	0.0036 0.0003	0.0152 0.0007	0.0031 0.0004	0.0102 0.0007	0.0055 0.0004	0.0017 0.0001	67.8775 2.1391	32.6525 1.5991	0.0038 0.0004
	cmcKO-Fasudil SEM	0.0035 0.0003	0.0175 0.0009	0.0036 0.0003	0.0131 0.0006	0.0070 0.0004	0.0031 0.0003	55.5460 3.4404	24.7720 1.9683	0.0038 0.0004
	cmcKO-Saline SEM	0.0032 0.0006	0.0158 0.0026	0.0031 0.0005	0.0118 0.0019	0.0066 0.0011	0.0029 0.0006	50.6606 8.7211	22.7046 4.1137	0.0036 0.0007
	p-value WT vs cKO	0.4390	0.0647	0.9133	0.0069	0.0029	0.0346	0.0044	0.0041	0.6616
4 Weeks	WT-Fasudil SEM	0.0034 0.0003	0.0173 0.0010	0.0032 0.0003	0.0120 0.0007	0.0068 0.0005	0.0026 0.0003	65.5200 1.2654	30.9580 0.8764	0.0045 0.0003
	p-value Baseline vs 4W	0.1731	0.0419	0.6962	0.2277	0.1285	0.7612	0.9258	0.9522	0.0977
	WT-Saline SEM	0.0032 0.0005	0.0150 0.0008	0.0029 0.0002	0.0104 0.0006	0.0050 0.0002	0.0017 0.0002	64.7750 1.0070	30.3450 0.6997	0.0032 0.0001
	p-value Baseline vs 4W	0.6045	0.7238	0.5379	0.4949	0.4890	0.8590	0.2120	0.2117	0.2558
	cmcKO-Fasudil SEM	0.0036 0.0003	0.0173 0.0008	0.0031 0.0002	0.0133 0.0005	0.0064 0.0005	0.0030 0.0003	53.0000 3.1926	23.2280 1.7103	0.0035 0.0004
	p-value Baseline vs 4W	0.7446	0.3887	0.3435	0.3304	0.0090	0.3337	0.3549	0.3536	0.3204
	cmcKO-Saline SEM	0.0031 0.0003	0.0176 0.0005	0.0029 0.0002	0.0142 0.0004	0.0082 0.0009	0.0046 0.0009	44.5500 5.6200	18.8950 2.8531	0.0036 0.0001
	p-value Baseline vs 4W	0.2214	0.0842	0.6275	0.0639	0.4938	0.1240	0.1827	0.1957	0.3698
p-value WT Saline vs Fasudil	0.9247	0.0387	0.8162	0.0024	0.0116	0.0233	0.0122	0.0080	0.0672	
p-value cKO Saline vs Fasudil	0.7807	0.9981	0.8366	0.1761	0.5866	0.3612	0.0065	0.0038	0.0827	
		LVD Mass ASE/ BW	IVRT msec	E m/s	e' m/s	E/e'	PAT msec	ET msec	PAT/ET	TVI cm
Baseline	WT-Fasudil SEM	0.0297 0.0017	10.6680 0.3683	0.8400 0.0475	0.0460 0.0060	19.6333 2.8415	20.1080 1.2891	57.4940 3.7072	35.3786 2.5844	1.8700 0.1727
	WT-Saline SEM	0.0276 0.0020	9.8875 0.4827	0.8925 0.0614	0.0450 0.0029	19.9625 1.3057	22.2700 1.8250	58.3625 2.3427	38.0623 2.1493	2.1325 0.1944
	cmcKO-Fasudil SEM	0.0308 0.0016	14.4460 0.5700	0.9200 0.0680	0.0300 0.0045	32.9833 4.2813	17.1400 1.8103	52.9360 2.7460	32.4109 3.1585	1.3960 0.1426
	cmcKO-Saline SEM	0.0271 0.0045	12.4015 2.1918	0.8680 0.1530	0.0286 0.0053	29.4483 5.3304	15.6255 2.8885	47.9093 7.9683	29.6675 5.0607	1.3508 0.2373
	p-value WT vs cKO	0.6408	0.0009	0.2123	0.0038	0.0008	0.0288	0.0827	0.1098	0.0060
4 Weeks	WT-Fasudil SEM	0.0301 0.0018	9.8840 0.6332	0.8220 0.0449	0.0380 0.0037	22.0767 1.2939	15.5560 1.2965	50.8800 2.1687	30.9007 3.1973	1.9720 0.1388
	p-value Baseline vs 4W	0.2628	0.4603	0.6198	0.3375	0.4641	0.1386	0.2669	0.4262	0.7531
	WT-Saline SEM	0.0278 0.0017	9.0025 0.6718	0.7800 0.0842	0.0325 0.0025	23.8958 1.2423	16.7650 0.9554	50.4775 3.9011	34.1109 4.1712	1.5900 0.1165
	p-value Baseline vs 4W	0.6799	0.2206	0.0272	0.0154	0.0648	0.1234	0.1105	0.5707	0.0221

cmcKO-Fasudil	0.0306	12.4140	0.9600	0.0280	36.4500	16.1680	44.2920	36.6407	1.1560
SEM	0.0016	1.2858	0.0674	0.0037	5.2192	1.0374	1.6690	2.5284	0.0604
p-value Baseline vs 4W	0.3034	0.2376	0.6077	0.7040	0.6906	0.7079	0.0858	0.3898	0.1666
cmcKO-Saline	0.0285	13.2200	0.9600	0.0275	36.0833	17.5275	48.0825	36.6870	1.4175
SEM	0.0018	1.0904	0.0280	0.0025	4.3999	0.8889	1.5983	2.7263	0.1521
p-value Baseline vs 4W	0.3448	0.6803	0.7601	0.1817	0.3725	0.7515	0.4933	0.1937	0.4379
p-value WT Saline vs Fasudil	0.7930	0.0165	0.0887	0.2070	0.0372	0.5803	0.5906	0.6237	0.4026
p-value cKO Saline vs Fasudil	0.8538	0.1155	0.1267	0.0955	0.0282	0.7220	0.0427	0.1967	0.0007

Table S5. Comparison of the Fasudil treatment between *Snrk* WT and Cardiomyocyte-conditional

SNRK null mice (*Snrk* cmcKO) – ECHO Analysis. ECHO was performed on 6-4 month adult male and female *Snrk* WT and cmcKO mice. The mice received daily injections of saline or fasudil as described in the materials and methods. Left ventricular dimensions were normalized to body weight (BW) g, interventricular septal end diastole (IVSd) cm, left ventricular internal diameter end diastole and end systole (LVIDd, LVIDs) cm, left ventricular posterior wall end diastole (LVPWd) cm, end diastolic volume (EDV), end systolic volume (ESV) parameters, ejection fraction (EF) %, fractional shortening (FS) %, left ventricular mass in diastole (LVD Mass ASE) g, stroke volume index (SVI) ml/g, isovolumic relaxation time (IVRT) msec, early mitral inflow velocity (E) m/s / early diastolic mitral annular velocity (e') m/s, pulmonary acceleration time (PAT) msec, ejection time (ET) msec and time-velocity integral (TVI) cm. There were 2 males and 2-3 females per experimental group.